Electronic Supplementary Material (ESI) for Energy & Environmental Science.


**Supplementary information**

# Design and evaluation of conjugated polymers with polar side chains as electrode materials for electrochemical energy storage in aqueous electrolytes

**Authors:**

**Authors:** Davide Moia,*[,a,‡] Alexander Giovannitti,*[,a,b,‡] Anna A. Szumska,[a] Iuliana P. Maria,[b] Elham Rezasoltani,[a] Michael Sachs,[b] Martin Schnurr,[b] Piers R.F. Barnes,[a] Iain McCulloch,[b,c] Jenny Nelson*[,a]

**Affiliations**

[a] Department of Physics, Imperial College London SW7 2AZ London, UK

[b] Department of Chemistry, Imperial College London SW7 2AZ London, UK

[c] Physical Sciences and Engineering Division, KAUST Solar Center (KSC), King Abdullah University of Science and Technology (KAUST), KSC Thuwal 23955-6900, Saudi Arabia

* d.moia@fkf.mpg.de; ag19@stanford.edu; jenny.nelson@imperial.ac.uk

[‡] These authors contributed equally to this work

# 1 Table of Contents


1 Table of Contents ..... 1
2 Material synthesis and characterization ..... 3
3 Summary of the synthesized materials and their properties ..... 4
3.1 Synthesis of p(gT2) ..... 4
3.2 Synthesis of p((DMA)-NDI-gT2) ..... 4
3.3 Synthesis of p(ZI-NDI-gT2) ..... 4
4 Monomer synthesis ..... 1
4.1 Synthesis of (DMA)-NDI-$Br_2$ ..... 1
4.2 Synthesis of 3,3'-bisalkoxy(TEG)-2,2'-bithiophene ..... 3
4.3 Synthesis of 5,5'-dibromo-3,3'- bisalkoxy(TEG)-2,2'-bithiophene ..... 4
4.4 Synthesis of (3,3'- bisalkoxy(TEG)-[2,2'-bithiophene]-5,5'-diyl)bis(trimethylstannane) ..... 6
5 Polymer synthesis ..... 8
5.1 Synthesis of p(gT2) ..... 8
5.2 Synthesis of p((DMA)-NDI-gT2) ..... 10
5.3 Synthesis of p((DMA-Br)-NDI-gT2) ..... 12
5.4 Synthesis of p(ZI-NDI-gT2) ..... 15
5.5 Synthesis of p(g7NDI-gT2) ..... 17
6 CV measurements in organic electrolytes ..... 19
7 UV Vis measurements ..... 21
8 Electrochemical and spectroelectrochemical measurements ..... 22
8.1 Sample preparation: ..... 22
8.2 Electrochemical measurements in aqueous electrolytes ..... 23
8.3 Spectroelectrochemical measurements in aqueous electrolytes ..... 23
9 Quantum chemical calculations ..... 24
9.1 p(gT2) ..... 25
9.2 n-type polymer - p(g7NDI-gT2) and p(ZI-NDI-gT2) ..... 27
10 Further electrochemical investigation and stability of p(gT2), p(ZI-NDI-gT2) and p(7NDI-gT2) 33
10.1 p(gT2) ..... 33
10.2 p(g7NDI-gT2) ..... 35
10.3 Stability of p(gT2), p(ZI-NDI-gT2) and p(g7NDI-gT2) ..... 36
10.4 Gravimetric capacity ..... 37
11 Charge density as a function of film thickness for the p-type and n-type polymers. ..... 38
12 Rate-capabilities of the p-type and n type polymers ..... 39
12.1 p(gT2) ..... 39
12.2 p(ZI-NDI-gT2) ..... 41

12.3 p(g7-NDI-gT2) ..... 43
13 Electrochemical cell ..... 44
13.1 Voltage of the electrochemical cell ..... 44
13.2 Electrochemical response of the two terminal electrochemical cell using films with different thicknesses ..... 44
13.3 Charge retention ..... 45
13.4 Hydrogen and oxygen detection ..... 46
13.5 Hydrogen peroxide detection ..... 47
13.6 Charging rate and stability of the electrochemical cell ..... 48
13.7 Capacity recovery ..... 49

# 2 Material synthesis and characterization

Column chromatography with silica gel from VWR Scientific was used for flash chromatography. Microwave experiments were carried out in a Biotage Initiator V 2.3. $^{1}H$ and $^{13}C$ NMR spectra were recorded on a Bruker AV-400 spectrometer at 298 K and are reported in ppm relative to TMS. UV-Vis absorption spectra were recorded on UV-1601 ($\lambda_{max}$ 1100 nm) UV-VIS Shimadzu spectrometers.

MALDI TOF spectrometry was carried out in positive reflection mode on a Micromass MALDImxTOF with trans-2-[3-(4-tert-Butylphenyl)-2-methyl-2-propenylidene]-malononitrile (DCTB) as the matrix.

Cyclic voltammograms were recorded on an Autolab PGSTAT101 with a standard three-electrode setup with ITO coated glass slides, a Pt counter electrode and a Ag/AgCl reference electrode (calibrated against ferrocene ($Fc/Fc^{+}$)). The measurements were either carried in an anhydrous, degassed 0.1 M tetrabutylammonium hexafluorophosphate ($TBAPF_6$) acetonitrile solution or in a 0.1 M NaCl aqueous solution as the supporting electrolyte with a scan rate of 100 mV/s. Ionisation potential were calculated according to the literature: IP [eV] = $E_{(Ox,onset\ vsFc/Fc+)}$+5.1.[1]

Gel permeation chromatography (GPC) measurements were performed on an Agilent 1260 infinity system operating in DMF with 5 mM $NH_4BF_4$ with 2 PLgel 5 μm mixed-C columns (300×7.5mm), a PLgel 5 mm guard column (50x7.5mm) at 50 °C with a refractive index detector as well as a variable wavelength detector. The instrument was calibrated with linear narrow poly(methyl methacrylate) standards in the range of 0.6 to 47kDa.

Dialysis was carried out in a dialysis kit Thermo Scientific Slide-A-Lyzer Cassette with a molecular weight cut off of 2K. The deionised water was replaced every 6 h and the dialysis was carried out for two days.

End-capping procedure: After the reaction was cooled to room temperature, 0.1 mL of a solution made of 1.00 mg of $Pd_2(dba)_3$ and 0.1 mL of 2-(Tributylstannyl)thiophene in 0.5 mL of anhydrous degassed DMF was added and heated for 1 h to 100 °C, then 0.1 mL of a solution made of 1.00 mg of $Pd_2(dba)_3$ and 0.1 mL of 2-bromothiophene in 0.5 mL of anhydrous degassed DMF was added and heated to 100 °C.

# 3 Summary of the synthesized materials and their properties

## 3.1 Synthesis of p(gT2)

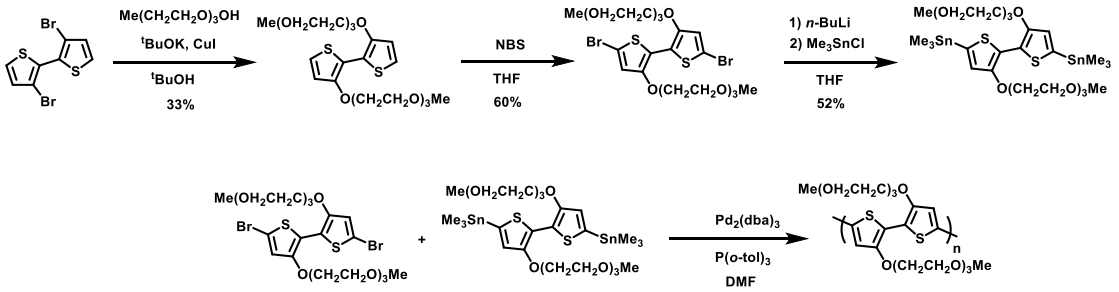


## 3.2 Synthesis of p((DMA)-NDI-gT2)

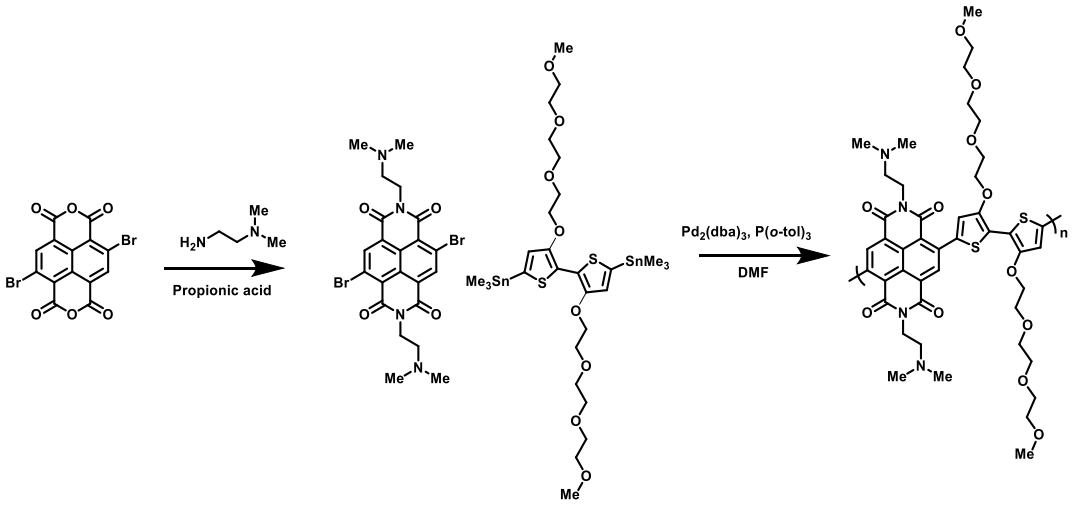


## 3.3 Synthesis of p(ZI-NDI-gT2)

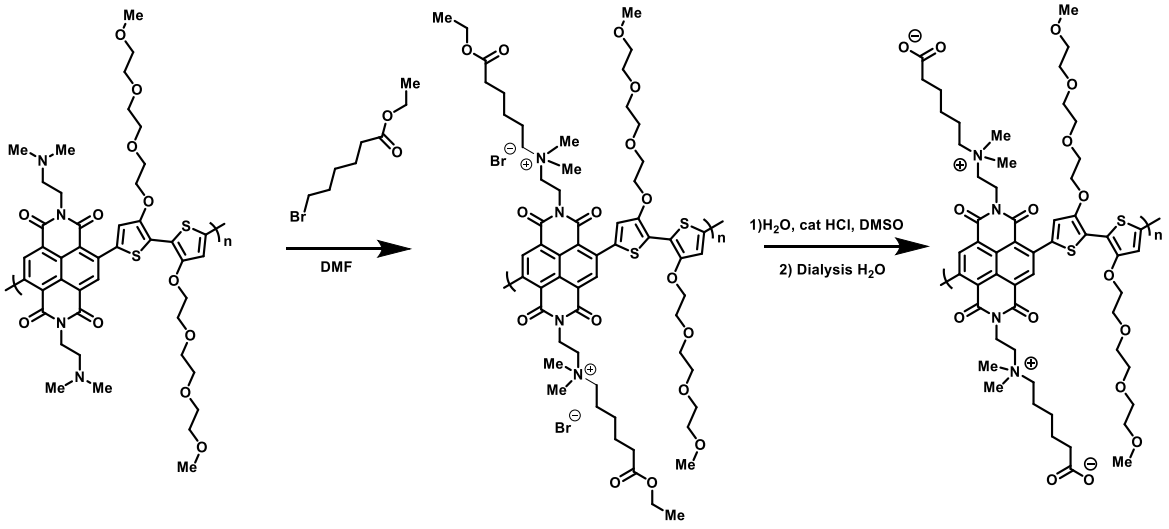

# 4 Monomer synthesis

## 4.1 Synthesis of (DMA)-NDI-$Br_2$

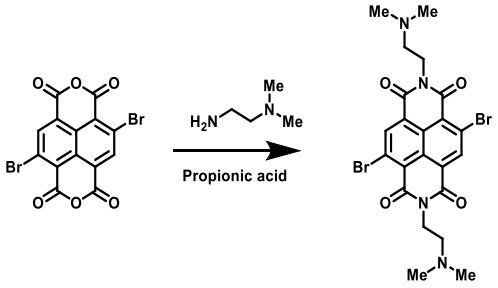


A 150 ml two neck round bottom flask was dried and purged with argon. 2,6-dibromonaphthalene-1,4,5,8-tetracarboxylic dianhydride (512 mg , 1.20 mmol, 1.0 eq.) was suspended in propionic acid (20 ml) and *N*,*N*-dimethylethane-1,2-diamine (0.23 mg, 2.33 mmol) was added. The reaction mixture was heated to 120°C for 2 h. The reaction was monitored by NMR and after full conversion of the starting material, 100 mL of water and 100 mL of chloroform were added (product is water soluble). The aqueous layer was first washed with chloroform (2 x 100 mL). Then, 200 mL of chloroform was added and a 2 M $NaHCO_3$ solution was added until a pH value of 8 - 9 was reached. The organic layer was washed with water (3 x 100 mL) and dried over MgSO4. The solvent was removed and the red solid was washed with methanol and acetone. Finally, the solid was washed with hot acetone and dried to obtain 250 mg (0.44 mmol) of an orange solid with a yield of 37 %.

$^{1}$H-NMR (400 MHz, trifluoroacetic acid -$d_1$) $\delta$: 9.00 (s, 2H), 4.68 (t, 4H), 3.68 (t, 4H), 3.13 (s, 12H) ppm. $^{13}$C-NMR (100 MHz, trifluoroacetic acid-$d_1$) $\delta$: 165.5, 142.5, 132.5, 130.2, 127.0, 126.6, 60.42, 46.3, 38.9 ppm. HRMS (ES-ToF): 565.0090 [M-$H^+$] (calc. 565.0086).

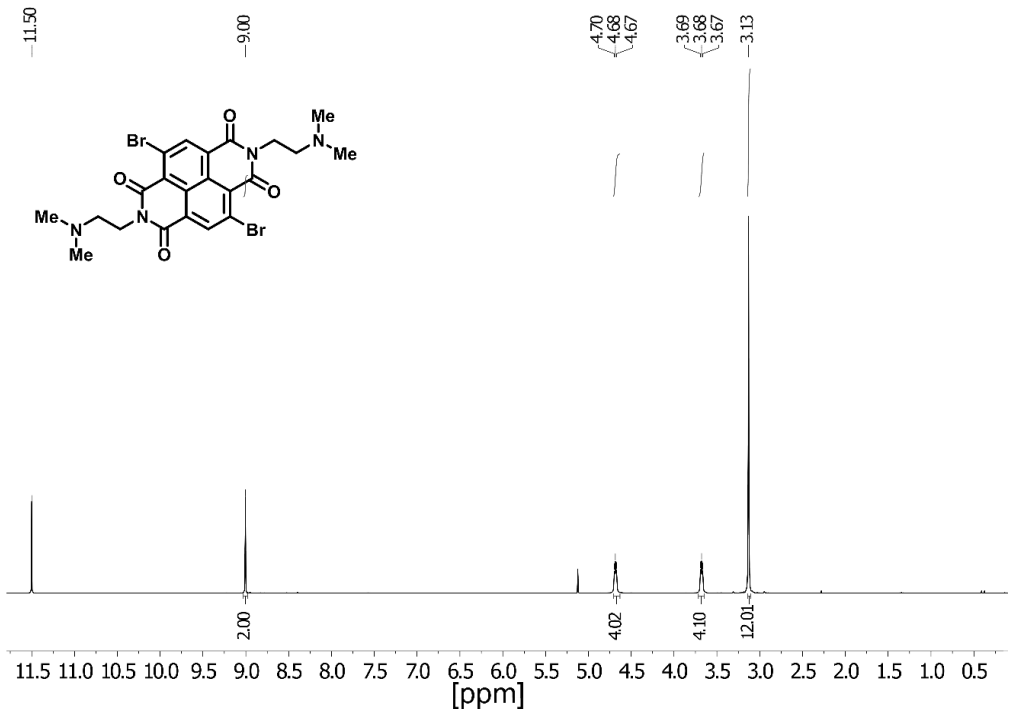


Figure S1. $^{1}$H NMR spectrum of (DMA)-NDI-$Br_2$ measured in TFA-$d_1$.

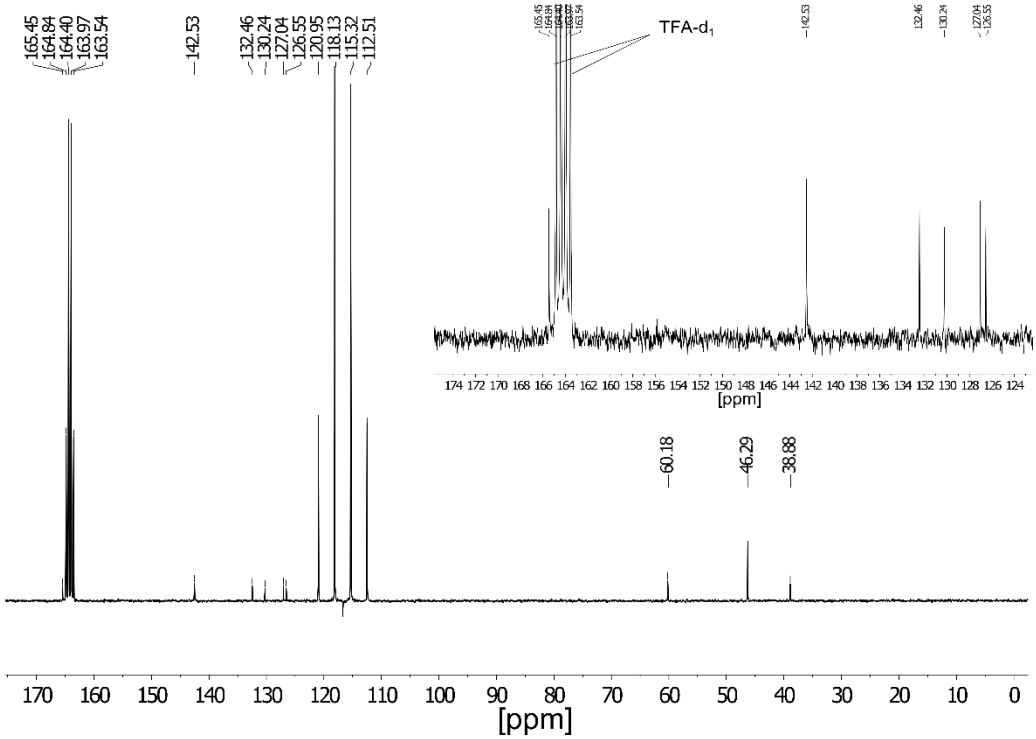


Figure S2. $^{13}$C NMR spectrum of (DMA)-NDI-$Br_2$ measured in TFA-$d_1$.

## 4.2 Synthesis of 3,3'-bisalkoxy(TEG)-2,2'-bithiophene

A 250 mL two neck RBF was dried and purged with argon. 3,3'-Dibromo-2,2'-bithiophene (6.48 g, 20 mmol), triethylene glycol monomethyl ether (11.5 g, 70 mmol), $^{t}$BuOK (6.73 g, 60 mmol) and CuI (1.52 g, 8.0 mmol) were suspended in anhydrous tert-butanol (100 mL). The reaction mixture was degassed with argon for 15 min and heated to reflux with stirring for 16 h. After the reaction was finished, water was added and the aqueous layer was extracted with ethyl acetate (200 mL). The organic phase was washed with DI water (3 x 100 mL), dried over $MgSO_4$ and concentrated *in vacuo* to afford the crude product as a dark yellow oil. Purification by column chromatography on silica gel with a solvent mixture of ethyl acetate : hexane 3:1 with 1 % of triethylamine afforded the target molecule as a yellow waxy solid (3.2 g, 6.52 mmol, 33% yield).

$^{1}$H NMR (400 MHz, $CDCl_3$) δ: 7.08 (d, *J* = 5.6 Hz, 2H), 6.85 (d, *J* = 5.6 Hz, 2H), 4.25 (t, *J* = 4.9 Hz, 4H), 3.90 (t, *J* = 5.0 Hz, 4H), 3.78 – 3.75 (m, 4H), 3.69 – 3.66 (m, 4H), 3.66 – 3.64 (m, 4H), 3.55 – 3.53 (m, 4H), 3.37 (s, 6H) ppm. $^{13}$C NMR (100 MHz, $CDCl_3$) δ: 151.9, 122.0, 116.7, 114.9, 72.1, 71.5, 71.1, 70.9, 70.7, 70.2, 59.2 ppm. HRMS (ES-ToF): 491.1774 [M-H$^+$] (calc. $C_{22}H_{35}O_8S_2$ 491.1773).

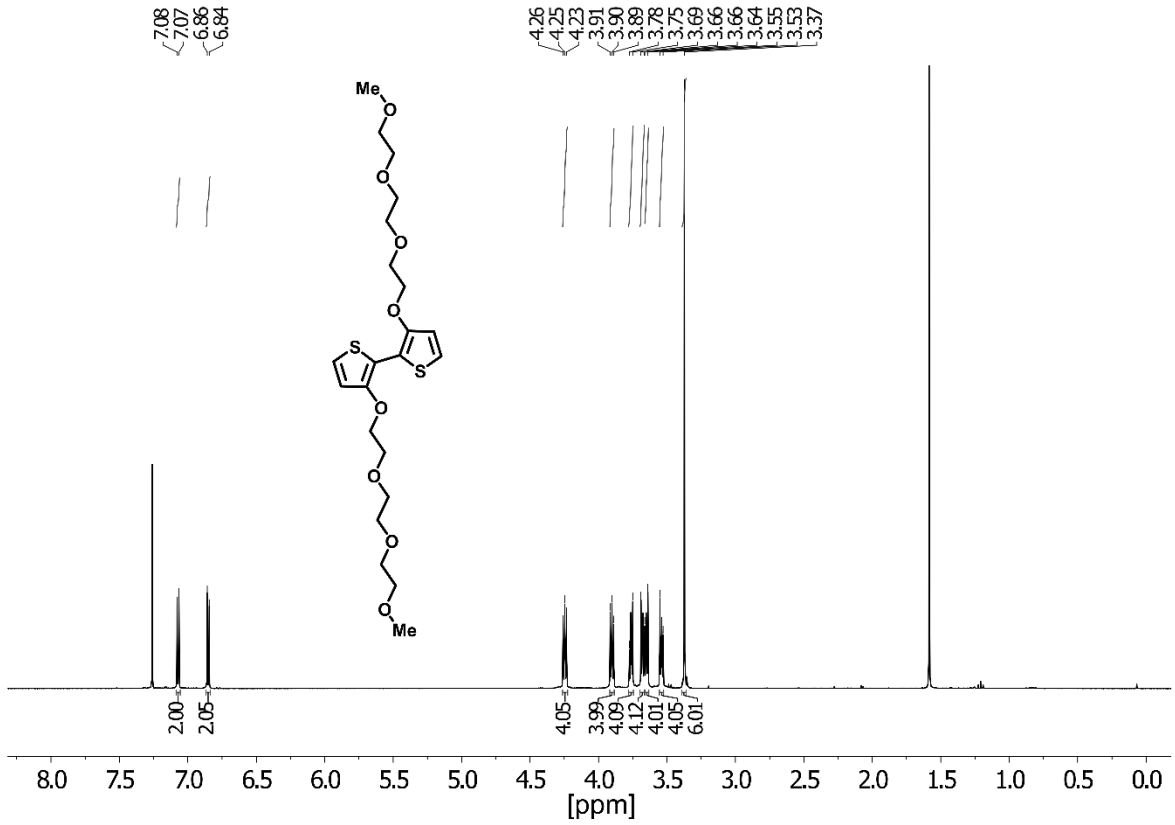


Figure S3. $^{1}$H NMR spectrum of 3,3'-bisalkoxy(TEG)-2,2'-bithiophene measured in $CDCl_3$.

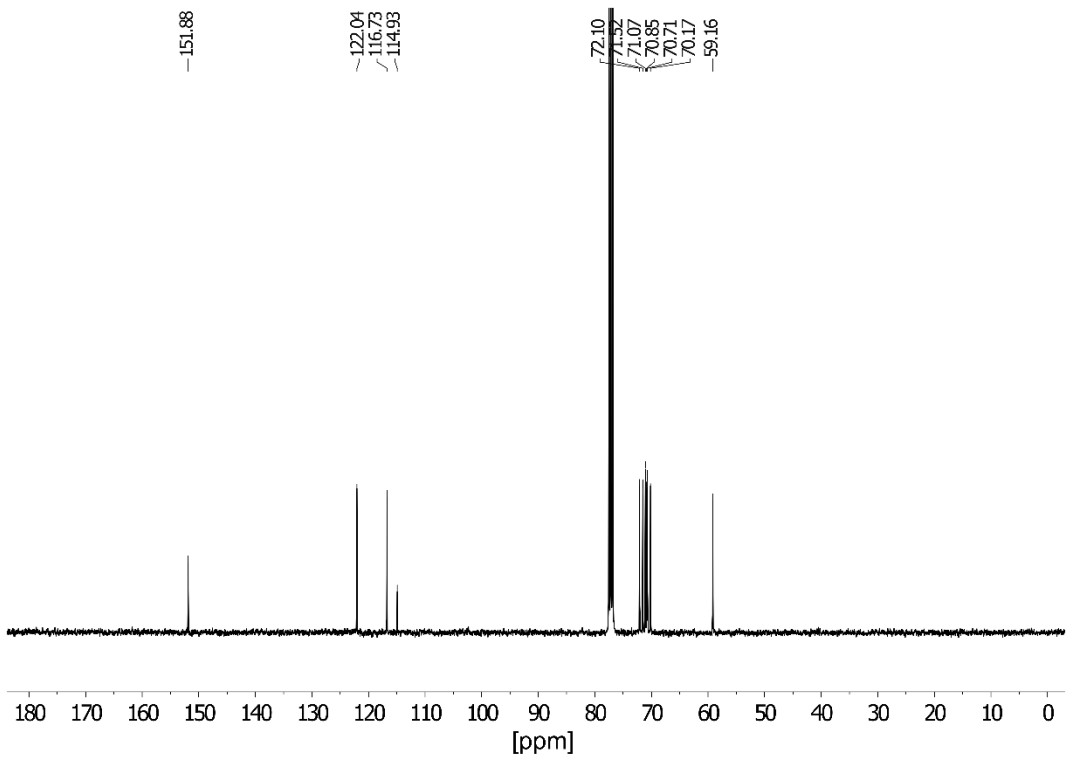


Figure S4. $^{13}C$ NMR spectrum of 3,3'-bisalkoxy(TEG)-2,2'-bithiophene measured in $CDCl_3$.

## 4.3 Synthesis of 5,5'-dibromo-3,3'- bisalkoxy(TEG)-2,2'-bithiophene

A protocol by Nielsen *et al.* was followed and slight modifications were carried out.[2] A two neck RBF was dried under vacuum and purged with argon. 3,3'-bisalkoxy(TEG)-2,2'-bithiophene (1.83 g. 2.24 mmol) was dissolved in anhydrous THF (200 mL), degassed with argon and cooled to - 20 °C. NBS (0.83 g, 4.66 mmol) was added in the dark and the reaction mixture was stirred for 10 min (reaction control indicated full conversion after 10 min). The reaction was quenched by the addition of 100 mL of 1 M $NaHCO_3$ aqueous solution, followed by the addition of 150 mL of ethyl acetate. The organic layer was washed with water (3 x 100 mL), dried over $MgSO_4$ and the solvent was removed under reduced pressure. Purification of the crude product was carried out by column chromatography on silica gel with a solvent mixture of hexane : ethyl acetate in the ration of 1 : 1 with 1 % of triethylamine. Finally, the product was recrystallised from diethyl ether/hexane to afford the product as a yellow solid with a yield of 60 %. (1.45 g, 2.24mmol).

$^1H$ NMR (400 MHz, $CDCl_3$) δ: 6.85 (s, 2H), 4.21 – 4.18 (m, 4H), 3.88 – 3.85 (m, 4H), 3.75 – 3.73 (m, 4H), 3.70 – 3.68 (m, 4H), 3.68 – 3.65 (m, 4H), 3.57 – 3.54 (m, 4H), 3.38 (s, 6H) ppm. $^{13}C$ NMR (100 MHz, $CDCl_3$) δ: 150.3, 119.8, 116.0, 111.2, 72.1, 71.8, 71.1, 70.9, 70.8, 70.3, 59.2 ppm. HRMS (ES-ToF): 646.9964 [M-$H^+$] (calc. $C_{22}H_{33}Br_2O_8S_2$ 646.9983).

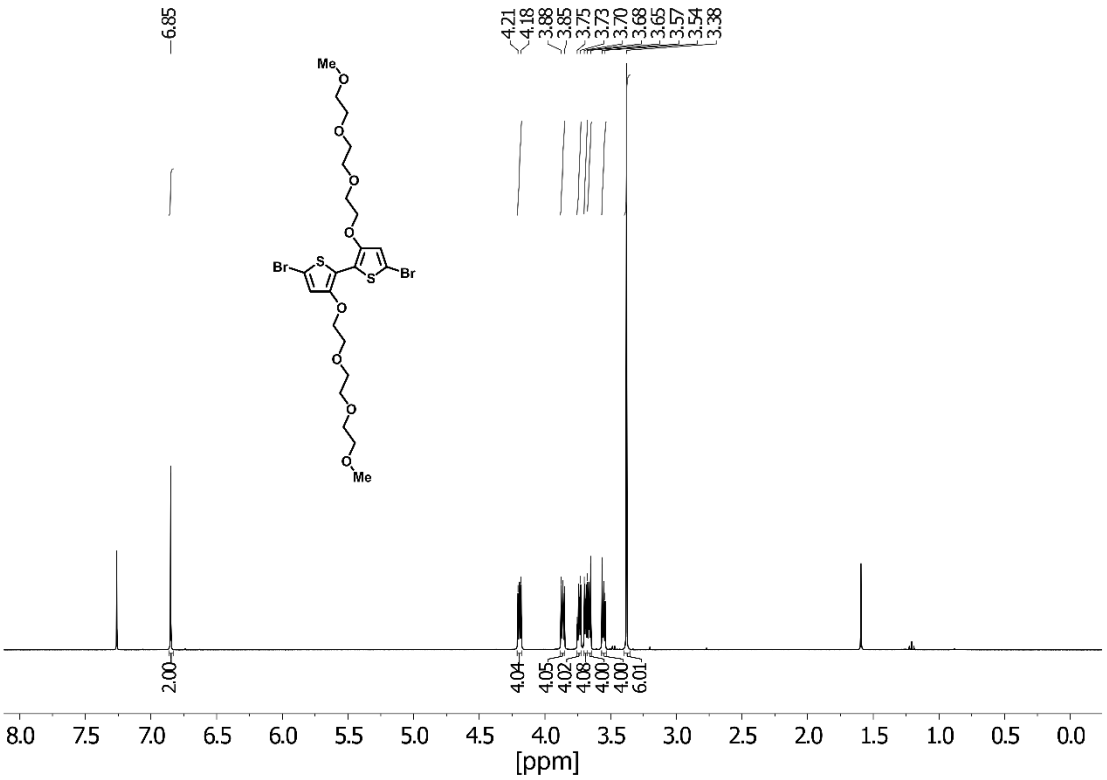


Figure S5. $^{1}H$ NMR spectrum of 5,5'-dibromo-3,3'- bisalkoxy(TEG)-2,2'-bithiophene measured in $CDCl_3$.

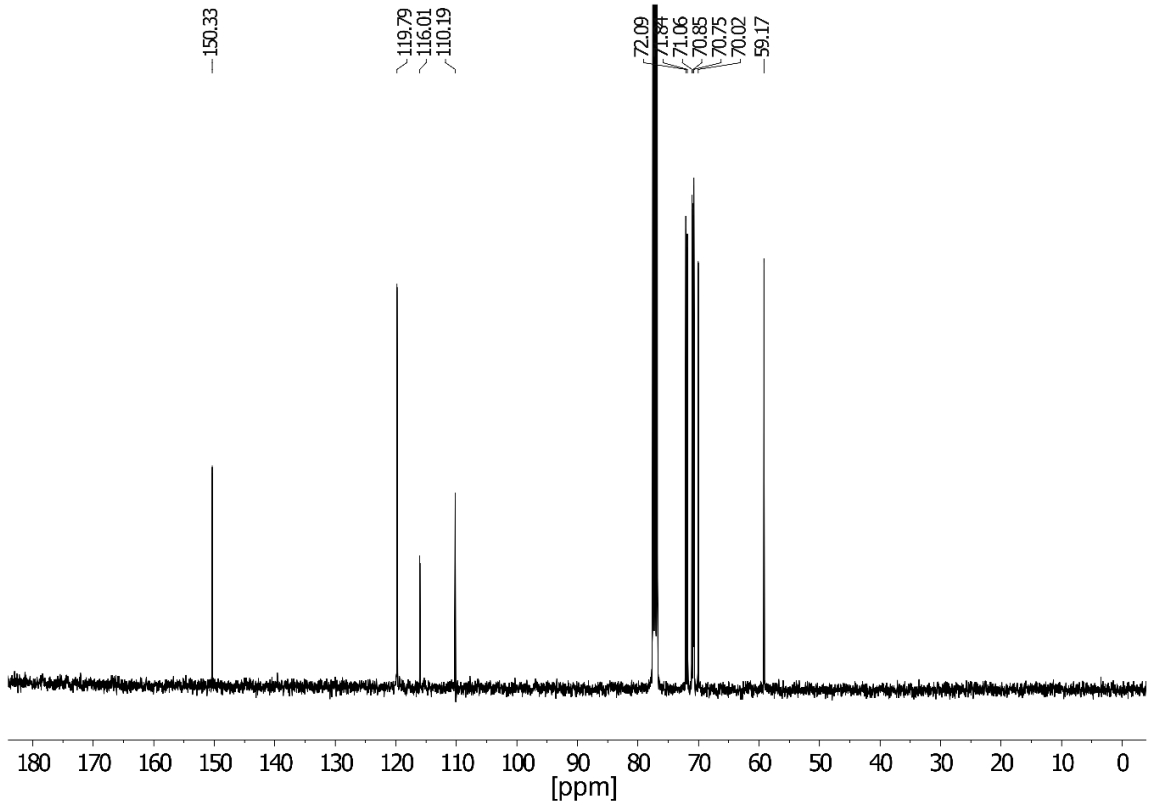


Figure S6. $^{13}C$ NMR spectrum of 5,5'-dibromo-3,3'- bisalkoxy(TEG)-2,2'-bithiophene measured in $CDCl_3$.

## 4.4 Synthesis of (3,3'- bisalkoxy(TEG)-[2,2'-bithiophene]-5,5'-diyl)bis(trimethylstannane)

A 250 mL two neck RBF was dried and purged with argon. 1.01 g of 5,5'-dibromo-3,3'-bisalkoxy(TEG)-2,2'-bithiophene (1.56 mmol, 1.0 eq.) was dissolved in 150 mL of anhydrous THF. The reaction mixture was cooled to -78 °C and 2.5 mL of *n*-BuLi (2.5 M in hexane, 6.23 mmol, 4.0 eq.) was added slowly. A yellow solution was formed which was stirred at -78 °C for 3 h. Then, 7.8 mL of trimethyltin chloride (1 M in hexane, 7.8 mmol, 5.0 eq.) was added and the reaction mixture was warmed to room temperature. 150 mL of diethyl ether was added and the organic phase was washed with water (3 x 100 mL) and dried over $Na_2SO_4$. The solvent was removed and the obtained solid was dissolved in 100 mL of acetonitrile which was washed with hexane (3 x 100 mL). The solvent was removed and the product was recrystallized from diethyl ether to obtain the product as yellow needles with a yield of 64 % (810 mg, 0.99 mmol).

$^1$H NMR (400 MHz, acetone-$d_6$) δ: 8.99 (s, 2H), 4.28 – 4.26 (m, 4H), 3.88 – 3.85 (m, 4H), 3.71 – 3.69 (m, 4H), 3.62 – 3.56 (m, 8H), 3.46 – 3.44 (m, 4H), 3.27 (s, 6H), 0.37 (s, 18 H) ppm. $^{13}$C NMR (100 MHz, acetone-$d_6$): 154.9, 134.9, 125.3, 121.1, 72.8, 72.4, 71.8, 71.3, 71.0, 59.0, 8.24 ppm. HRMS (ES-ToF): 819.1069 [M-H+] (calc. 819.1084).

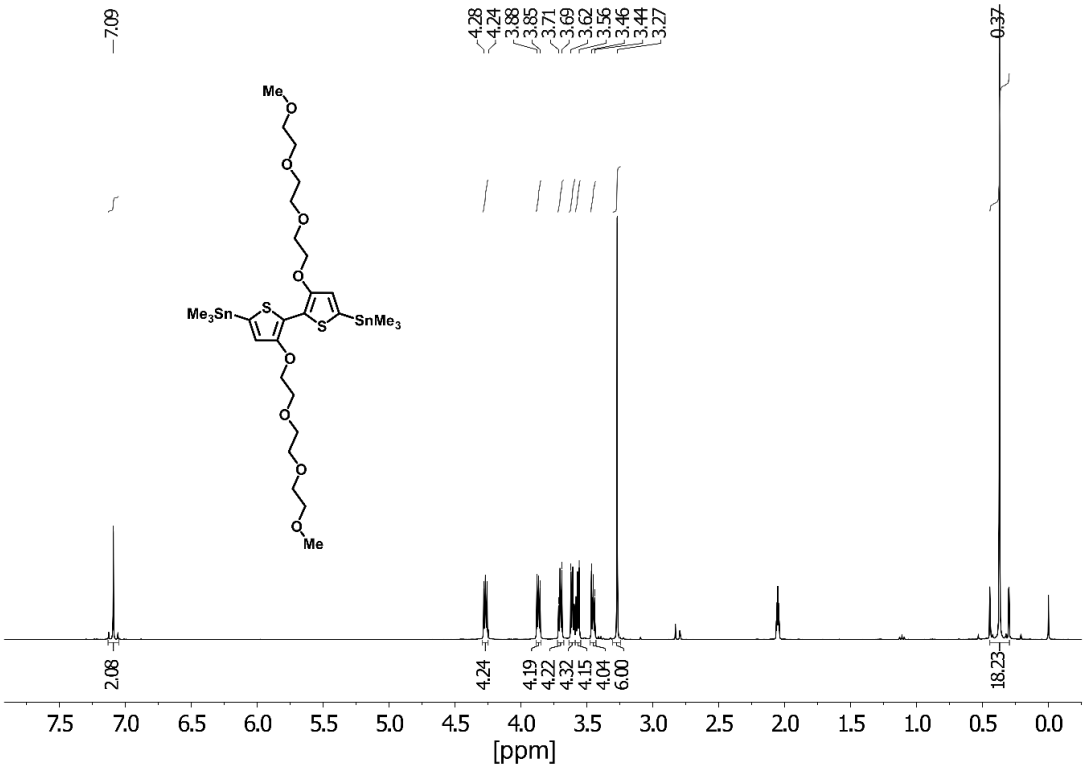


Figure S7. $^1$H NMR spectrum of (3,3'- bisalkoxy(TEG)-[2,2'-bithiophene]-5,5'-diyl)bis(trimethylstannane) in acetone-$d_6$.

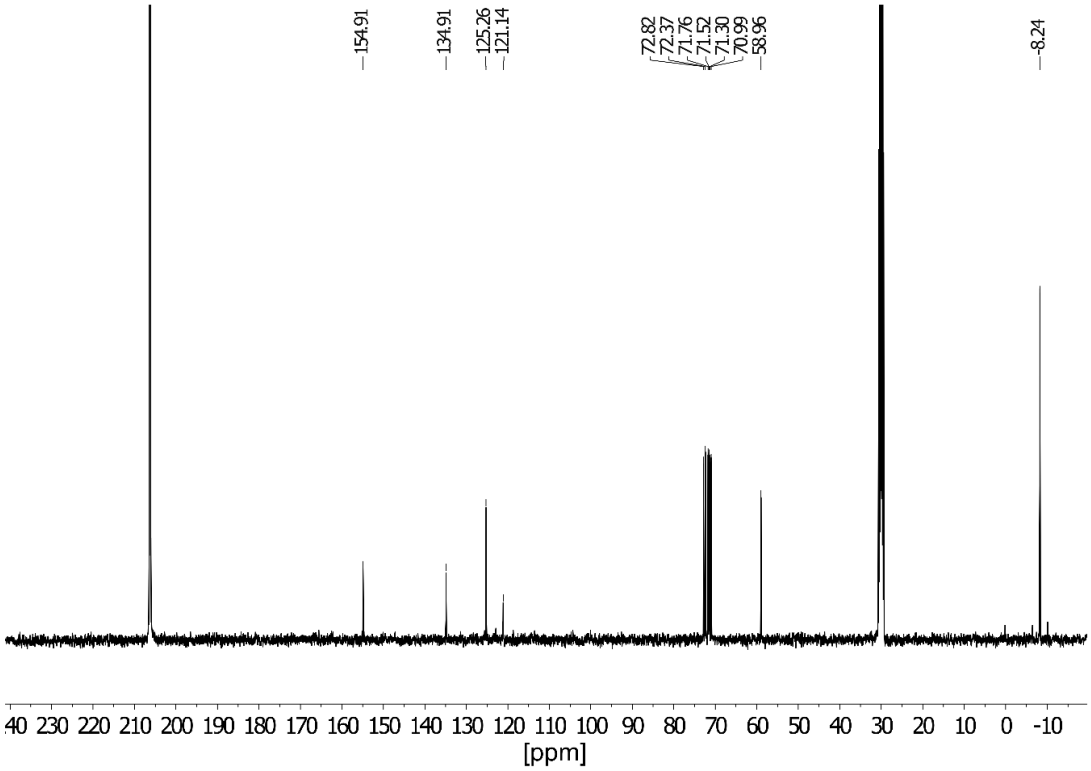


Figure S8. $^{13}C$ NMR spectra of (3,3'- bisalkoxy(TEG)-[2,2'-bithiophene]-5,5'-diyl)bis(trimethylstannane) in acetone-$d_6$.

# 5 Polymer synthesis

## 5.1 Synthesis of p(gT2)

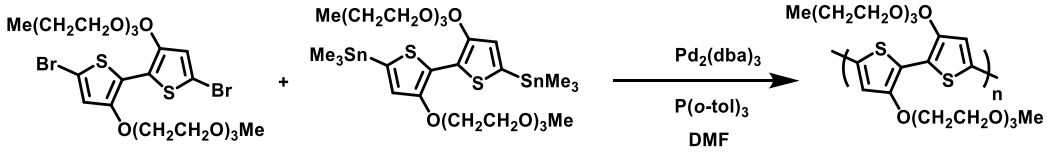


In a dried 5.0 mL microwave vial, 79.4 mg of (3,3'- bisalkoxy(TEG)-[2,2'-bithiophene]-5,5'-diyl)bis(trimethylstannane) (97.3 µmol) and 63.1 mg of 5,5'-dibromo-3,3'- bisalkoxy(TEG)-2,2'-bithiophene (97.3 µmol) were dissolved in 3.0 mL of anhydrous, degassed DMF. $Pd_2(dba)_3$ (1.78 mg, 1.95 µmol) and P(*o*-tol)$_3$ (2.37 mg, 7.78 µmol) were added and the vial was sealed and heated to 100 °C for 16 h. After the polymerization has finished, the end-capping procedure was carried out. Then, the reaction mixture was cooled to room temperature and precipitated in methanol. A blue solid was formed which was filtered into a glass fibre-thimble and Soxhlet extraction was carried out with methanol, ethyl acetate, acetone, hexane, and chloroform. The polymer dissolved in hot chloroform. Finally, the polymer was dissolved in a minimum amount of chloroform and precipitated in methanol. The collect solid was filtered and dried under high vacuum. A blue solid was obtained with a yield of 74 % (70 mg, 71.6 µmol).

GPC (DMF, 50 °C) $M_n$ = 36 kDa, $M_w$ = 60 kDa (including the first fraction $M_n$ = 56 kDa, $M_w$ = 306 kDa).$^1$H NMR ($CDCl_3$, 400 MHz) δ: 6.96 (br s, 2 H), 4.35 (br s, 4 H), 4.01 – 3.92 (m, 4 H), 3.81 – 3.79 (m, 4 H), 3.72 – 3.70 (m, 4 H), 3.66 – 3.63 (m, 4 H), 3.53 – 3.50 (m, 4 H), 3.34 (s, 6 H) ppm.

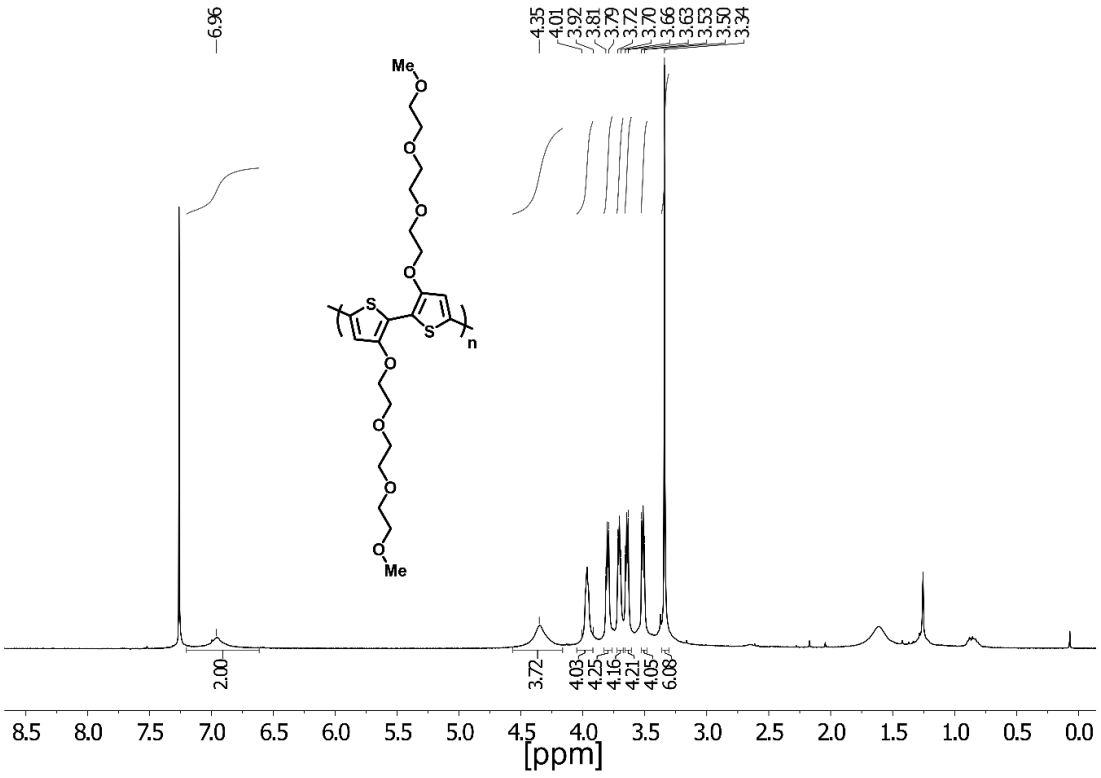


Figure S9. $^1$H NMR spectrum of p(gT2) in $CDCl_3$ at 25 °C.

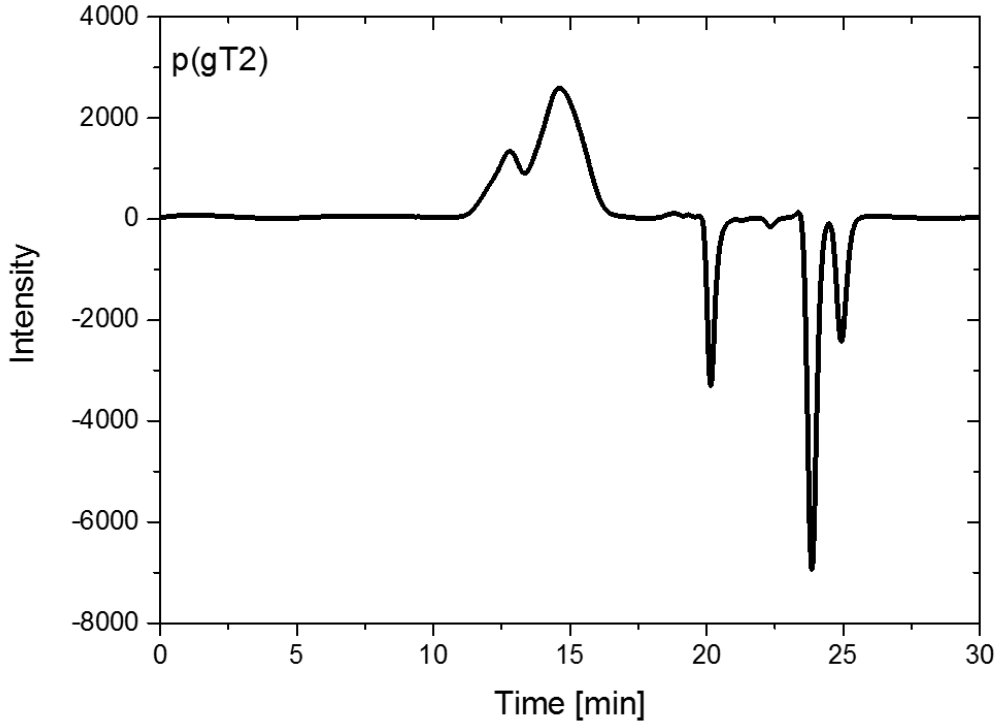


Figure S10: GPC measurements of p(gT2) in DMF (bimoduale eluation).

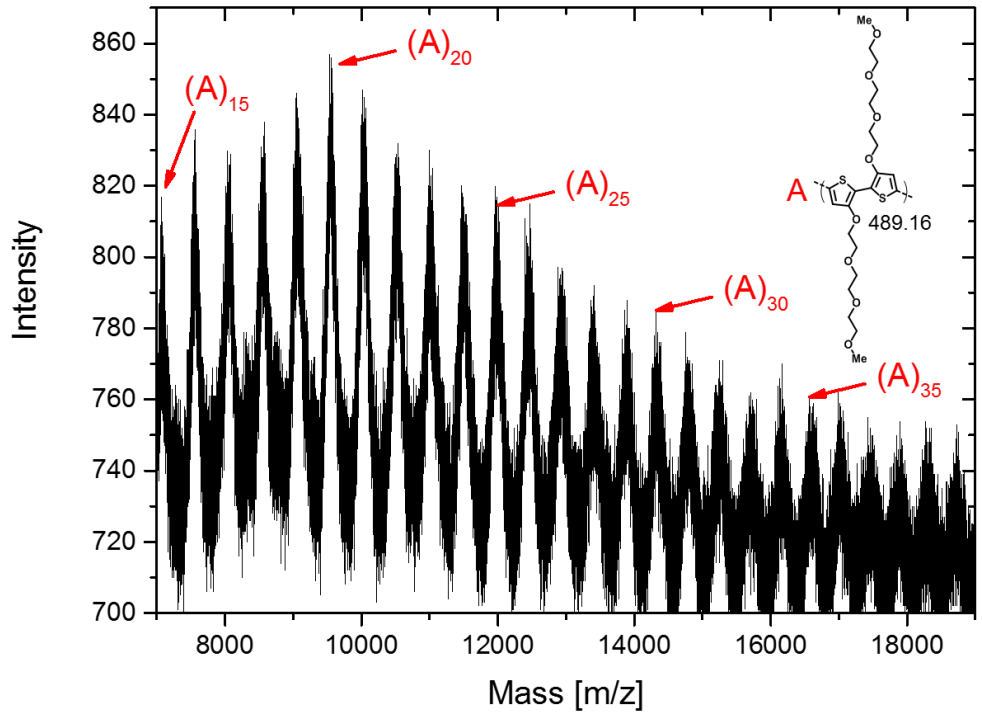


Figure S11. MALDI-ToF spectrum of p(gT2), measured in positive linear mode with DCTB as the matrix.

## 5.2 Synthesis of p((DMA)-NDI-gT2)

In a 5.0 mL microwave vial, 38.76 mg of (DMA)-NDI-$Br_2$ (68.45 µmol, 1.0 eq.), 55.86 mg of (3,3'-bisalkoxy(TEG)-[2,2'-bithiophene]-5,5'-diyl)bis(trimethylstannane) (68.45 µmol, 1.0 eq.), 1.4 mg of $Pd_2(dba)_3$ (1.52 µmol, 2 mol%) and 1.87 mg of P(*o*-tol)$_3$ (6.12 µmol, 8 mol%) were dissolved in 1.5 mL of anhydrous, degassed DMF and the vial was heated to 85 °C for 16 h. The color changed from yellow to dark green. After the polymerization has finished, the end-capping procedure was carried out. Then, the reaction mixture was cooled to room temperature and the reaction mixture was precipitated in ethyl acetate. The precipitate was filtered and Soxhlet extraction was carried out with ethyl acetate, methanol, acetone, hexane and chloroform. The polymer was soluble in hot chloroform. Polymer p((DMA)-NDI-gT2) was obtained as a green solid with a yield of 79 % (48.4 mg, 54.1 µmol).

GPC ($CHCl_3$, 50 °C) $M_n$ = 5.3 kDa, $M_w$ = 8.9 kDa. $^1$H-NMR (400 MHz, $CHCl_3$) δ: 8.82 (br s, 2H), 7.26 (br s, 4H), 4.42 (br s, 4H), 4.35 (br s, 4H), 4.26 (br s, 4H), 3.91 − 383 (m, 4H), 3.83 – 3.75 (m, 4H), 3.75 – 3.64 (m, 4H), 3.64 – 3.54 (m, 4H), 3.54 – 3.45 (m, 4H), 3.39 – 3.28 (m, 6H), 2.69 – 2.58 (m, 4H), 2.40 – 2.22 (m, 12H) ppm.

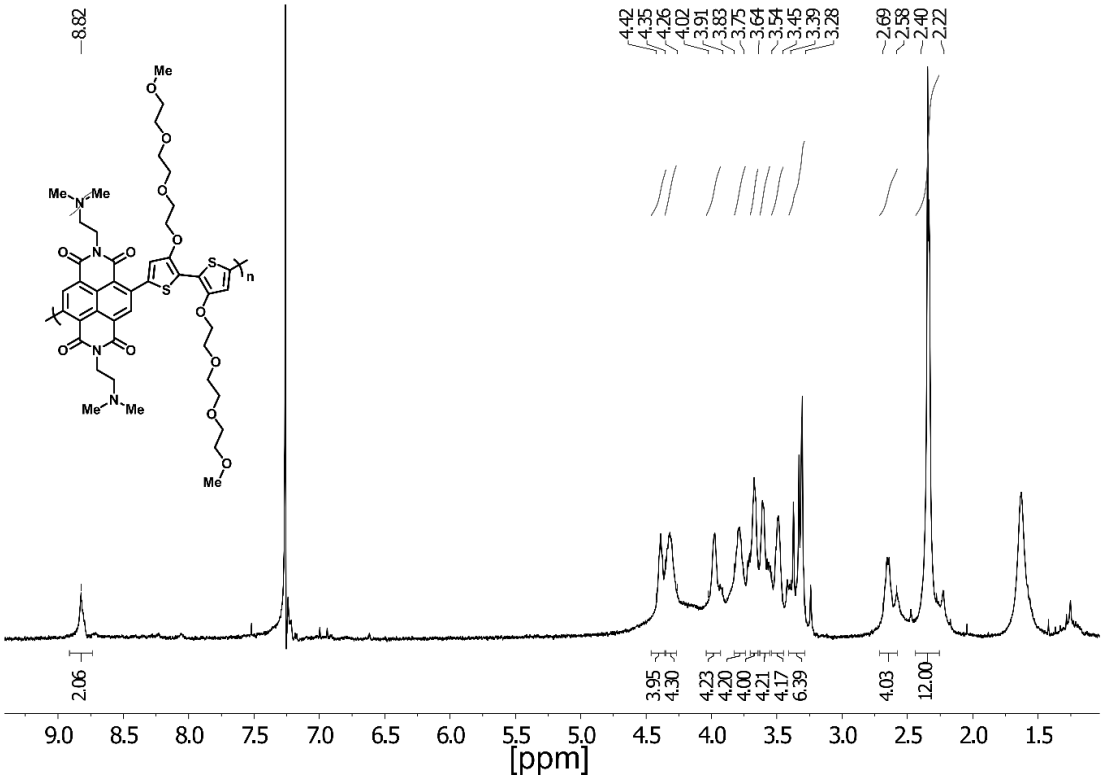


Figure S12. $^1$H NMR spectrum of p((DMA)-NDI-gT2) in $CDCl_3$ at 25 °C.

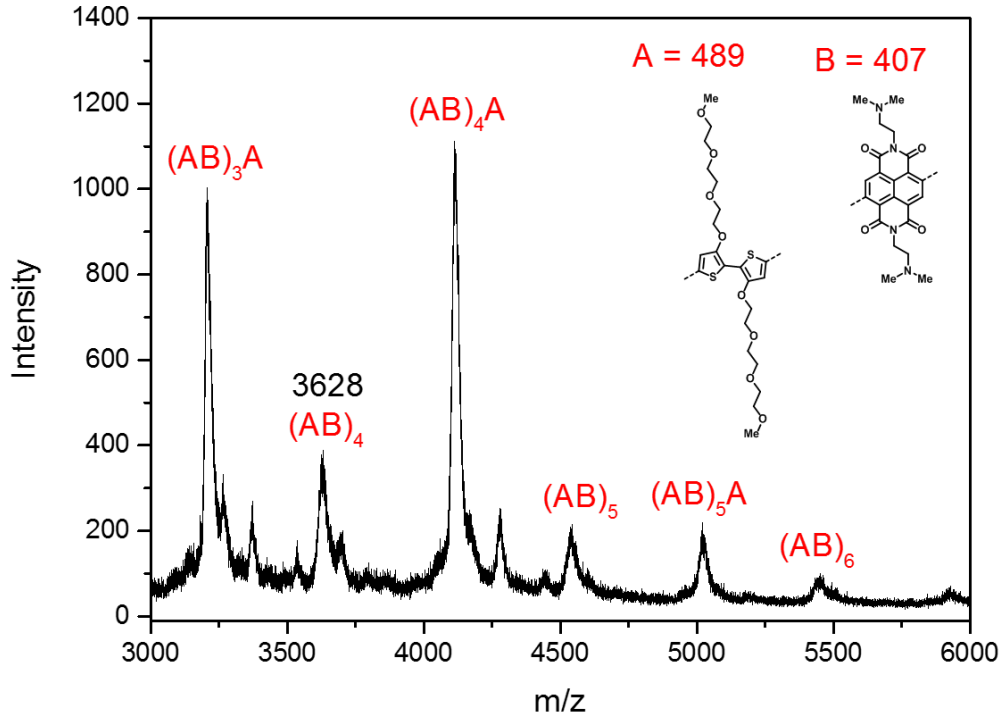


Figure S13. MALDI-ToF spectrum of p((DMA)-NDI-gT2).

## 5.3 Synthesis of p((DMA-Br)-NDI-gT2)

A 5.0 mL microwave vial was dried and purged with argon, 14.3 mg p((DMA)-NDI-gT2) (15.9 µmol) was suspended in 4.00 ml anhydrous DMF and 0.5 ml ethyl-6-bromohexanoate (2.8 mmol) was added. The reaction mixture was heated to 120°C for 1.5 h and a green solution was formed. The reaction mixture was cooled to room temperature and the solvent was removed under reduced pressure. The green solid was suspended in 3 mL of methanol and precipitated in acetone followed by the addition of hexane. The solution was filtered and the green solid was washed with chloroform and acetone. Finally, the polymer was dried under high vacuum for 16 h. 20.6 mg (15.4 µmol) of the polymer was obtained as a green solid with a yield 97%.

GPC (DMF, 50 °C) $M_n$ = 38 kDa, $M_w$ = 60 kDa. $^1$H-NMR (500 MHz, DMSO-$d_6$) δ: 8.64 – 8.57 (m, 2H), 7.81 – 7.48 (m, 4H), 4.49 – 4.24 (m, 8H, signals overlapping), 4.07 – 3.98 (m, 4H, $COCH_2$), 3.98 – 3.89 (m, 4H), 3.68 – 3.62 (m, 4H), 3.57 – 3.50 (m, 8H), 3.47 – 3.40 (m, 8H), 3.22 – 3.11 (m, 12H), 2.95 – 2.86 (m, 4H), 3.98 – 3.89 (m, 4H), 2.37 – 2.29 (m, 4H), 1.80 – 1.70 (m, 4H), 1.62 – 1.54 (m, 4H), 1.37 – 1.27 (m, 4H), 1.18 – 1.13 (m, 6H) ppm.

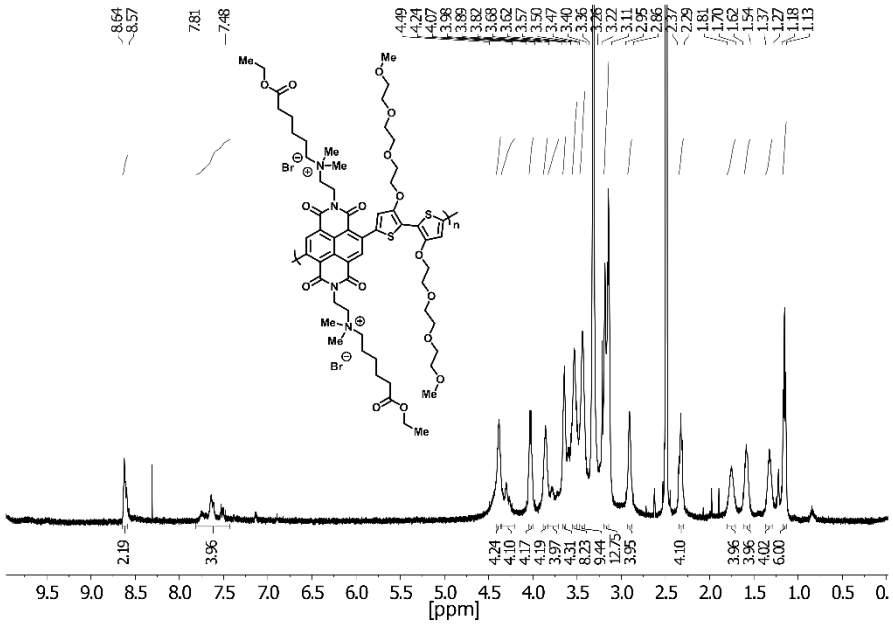


Figure S14. $^1$H NMR spectrum of p((DMA-Br)-NDI-gT2)in DMSO-$d_6$ at 22 °C.

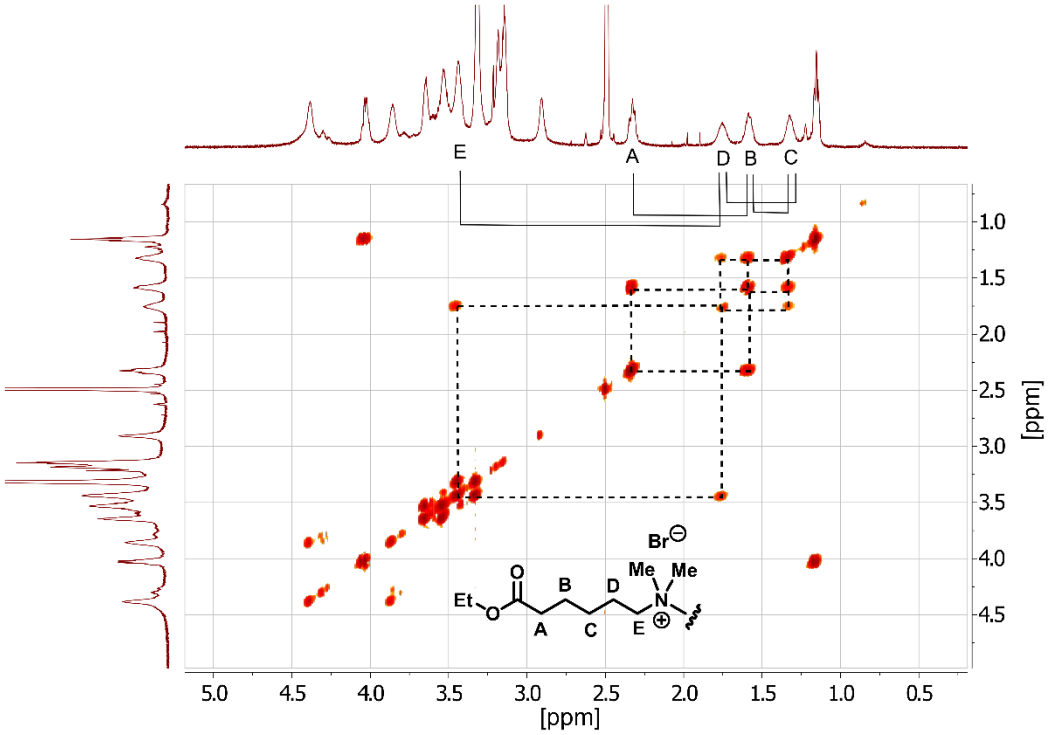


Figure S15. 2D COSY spectrum of p((DMA-Br)-NDI-gT2) in DMSO-$d_6$ at 25 °C, proton couplings of the alkylation are highlighted.

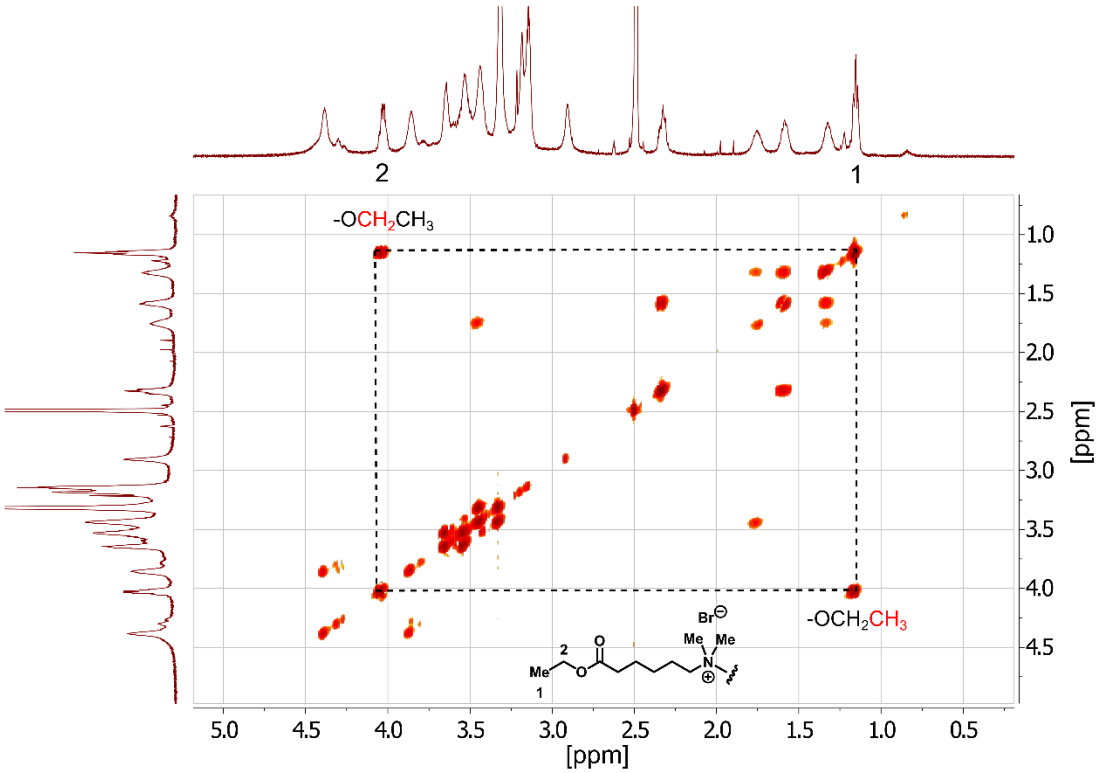


Figure S16. 2D COSY spectrum of p((DMA-Br)-NDI-gT2) in DMSO-$d_6$ at 25 °C, proton couplings of ester group are highlighted.

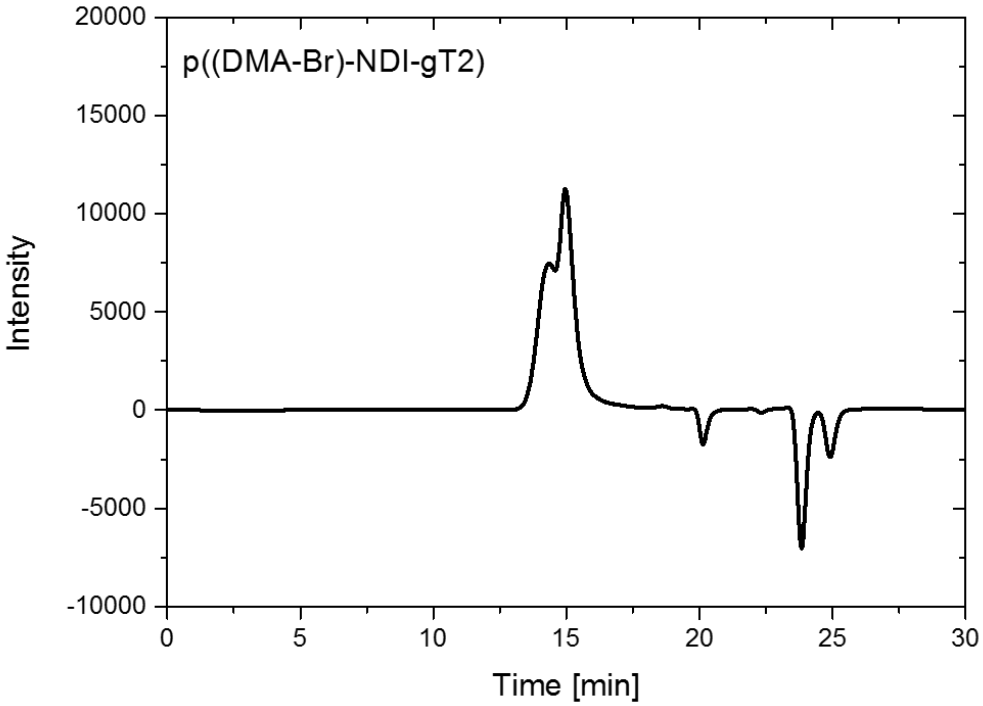


Figure S17. GPC measurements of p((DMO-Br)-NDI-gT2) in DMF (bimoduale eluation).

## 5.4 Synthesis of p(ZI-NDI-gT2)

In a 7.0 mL microwave, 10 mg of p((DMA-Br)-NDI-gT2) (8.46 µmol, 1.00 eq.) was dissolved in 2 mL of DMSO and 2 mL of water. 0.1 mL of conc. HCl was added and the reaction mixture was heated to 75 °C for 16 h. Then, the reaction mixture was cooled to room temperature and the solution was transferred into a dialyses kit (molecular weight cut off 2kDa) and the dialysis kit was stirred in DI water for 2 days, exchanging the water every 6 h. Finally, solvent was removed and the polymer was dried at 60 °C for 16 h. 9.2 mg (8.19 µmol) of a green polymer was obtained with a yield of 97 %.

GPC (DMF, 50 °C) $M_n$ = 24 kDa, $M_w$ = 53 kDa. $^1$H-NMR (500 MHz, DMSO-$d_6$) δ: 8.67 – 8.55 (m, 2H), 7.73 – 7.45 (m, 4H), 4.48 – 4.30 (m, 8H, signals overlapping), 3.61 – 3.56 (m, 8H, signals overlapping), 3.55 – 3.52 (m, 4H), 3.46 – 3.40 (m, 8H), 3.40 – 3.24 (m, 4H, overlap with water peak), 3.23 – 3.12 (m, 12H), 2.30 – 2.21 (m, 4H), 1.81 – 1.70 (m, 4H), 1.62 – 1.54 (m, 4H), 1.37 – 1.28 (m, 4H) ppm.

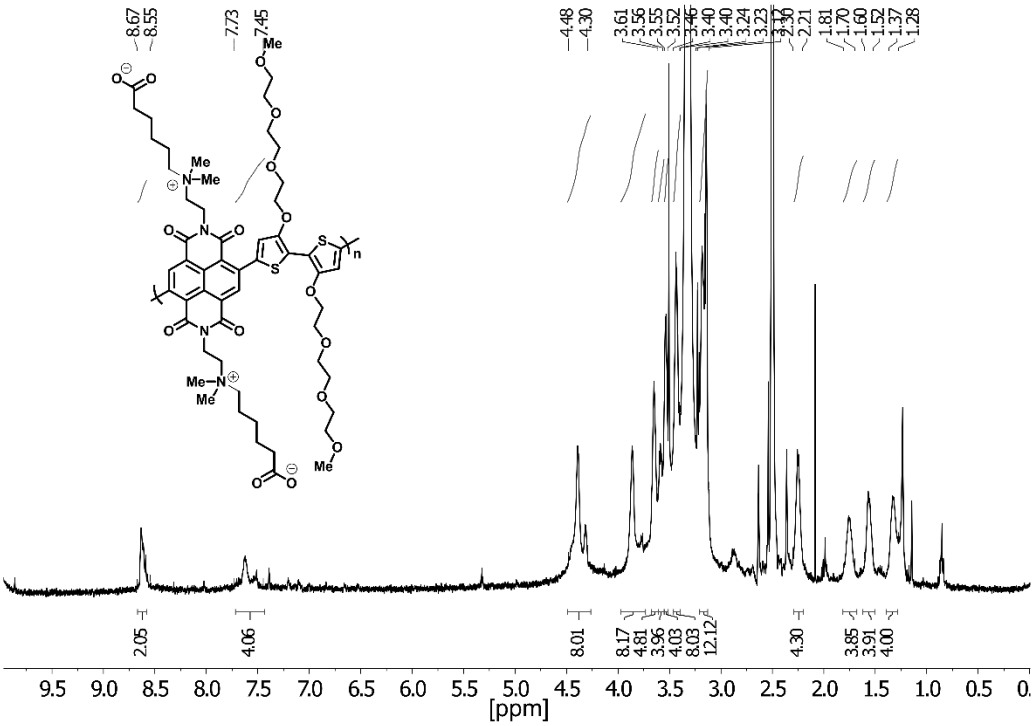


Figure S18. $^1$H NMR spectrum of p(ZI-NDI-gT2) in DMSO-$d_6$.

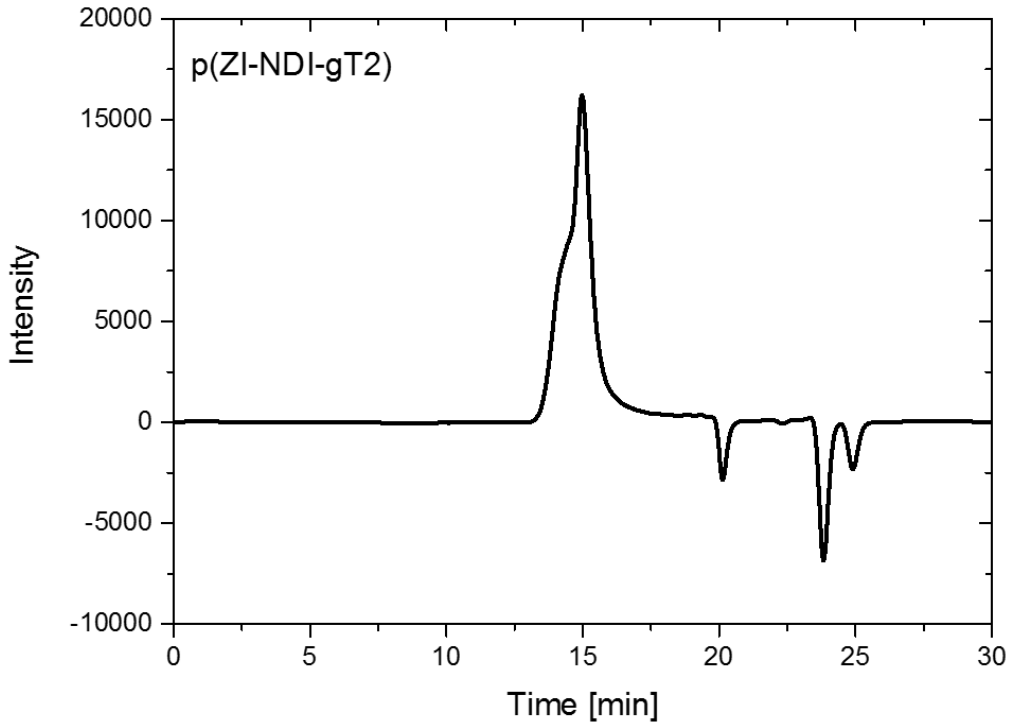


Figure S19. GPC of p(ZI-NDI-gT2) in DMF (bimoduale eluation).

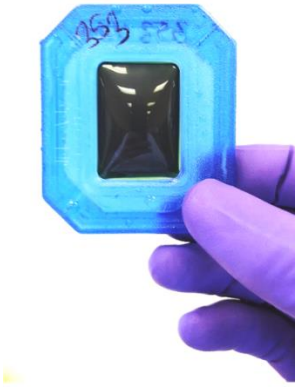

Figure S20. Dialysis of p(ZI-NDI-gT2) in DI water.

## 5.5 Synthesis of p(g7NDI-gT2)

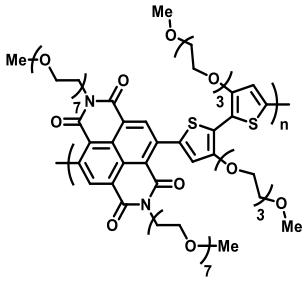

In a 7.0 mL microwave vial, 72.25 mg of g7NDI-$Br_2$ (67.6 µmol, 1.0 eq.) and 55.17 mg of (3,3'-bisalkoxy(TEG)-[2,2'-bithiophene]-5,5'-diyl)bis(trimethylstannane) (67.6 µmol, 1.0 eq.) were dissolved in 2.0 mL of anhydrous, degassed chlorobenzene. 1.36 mg of $Pd_2(dba)_3$ (1.35 µmol, 2 mol%) and 1.78 mg of P(*o*-tol)$_3$ (5.4 µmol, 8 mol%) were added and the vial was heated to 135 °C for 16 h. After the polymerization has finished, the end-capping procedure was carried out. Then, the reaction mixture was cooled to room temperature and the dark green reaction mixture was precipitated in ethyl acetate followed by addition of hexane. Soxhlet extraction was carried out with hexane, ethyl acetate, MeOH, acetone, THF and chloroform. The polymer was soluble in hot chloroform. Polymer p(g7NDI-gT2) was obtained as a dark green solid with a yield of 76 % (48 mg, 0.05 mmol).

GPC ($CHCl_3$:DMF; 5:1, 50 °C) $M_n$ = 14 kDa, $M_w$ = 26 kDa. $^1$H NMR (400 MHz, $CDCl_3$) δ: 8.82 (s, 2H), 7.31 – 7.16 (m, 4H), 4.44 – 4.34 (m, 4H), 4.34 – 4.25 (m, 4H), 4.02 – 3.93 (m, 4H), 3.89 – 3.75 (m, 4H), 7.31 – 7.16 (m, 4H), 3.70 – 3.52 (m, 60H), 3.52 – 3.49 (m, 4H), 3.36 (br s, 12H).

CV (PESA) = 5.1 eV

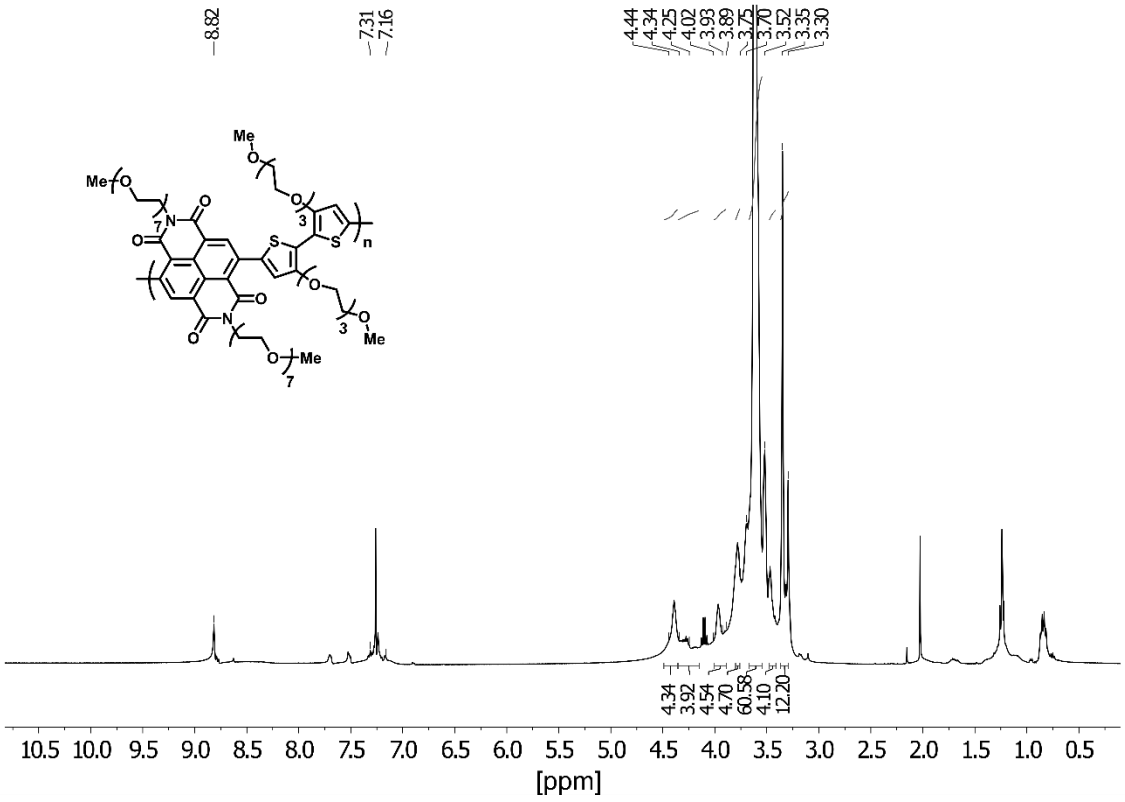


Figure S21. $^1$H NMR spectrum of polymer p(g7NDI-gT2) in $CDCl_3$ at 22 °C, aromatic signals were not integrated due to the overlap with the solvent peak.

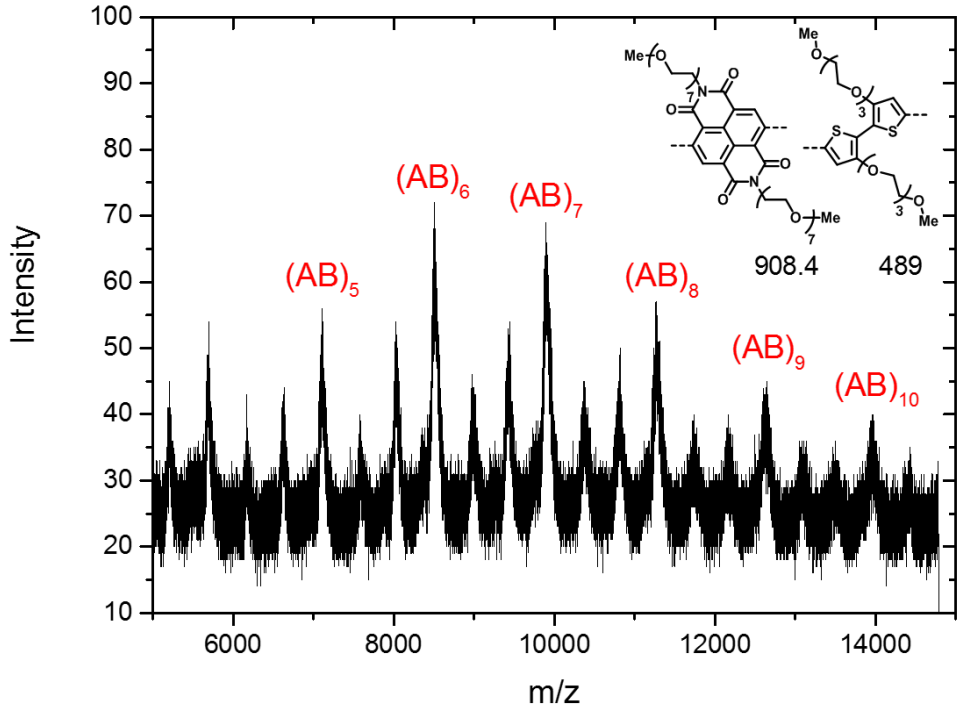


Figure S22. MALDI-ToF mass spectrum of p(g7NDI-gT2)

# 6 CV measurements in organic electrolytes

Thin film CV measurements reported in this section and in Figure 2b in the main text were carried out on FTO coated glass substrates with a 0.1 M $TBAPF_6$ acetonitrile solution as the supporting electrolyte. Potentials are reported vs Ag/AgCl and the scan rate of the measurement was 100 mV/s. The oxidation of ferrocene (solution) was used as the reference to calculate IP and EA values ($E_{1/2}$ ($Fc/Fc^+$) = 0.46 V vs Ag/AgCl)

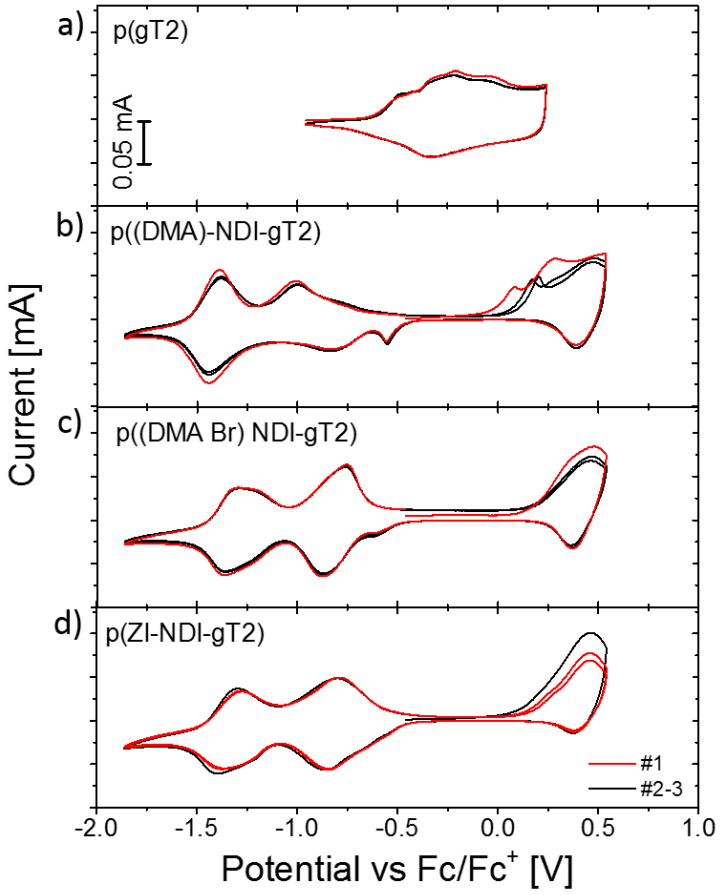


Figure S23: CV measurements of a) p(gT2), b) p((DMA)-NDI-gT2), c) p((DMA-Br)-NDI-gT2), d) p(ZI-NDI-gT2) with a degassed 0.1 M $NBu_4PF_6$ acetonitrile solution as the supportive electrolyte.

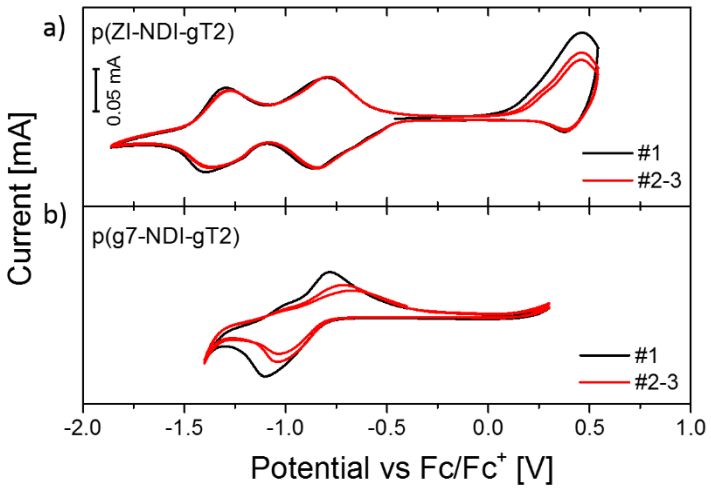


Figure S24: CV of a) p(ZI-gNDI-gT2) and b) p(g7-NDI-gT2) with a degassed 0.1 M $NBu_4PF_6$ acetonitrile solution as the supportive electrolyte. Polymer p(g7-NDI-gT2) showed limited redox-stability where applying higher voltages results in irreversible charging.

# 7 UV Vis measurements

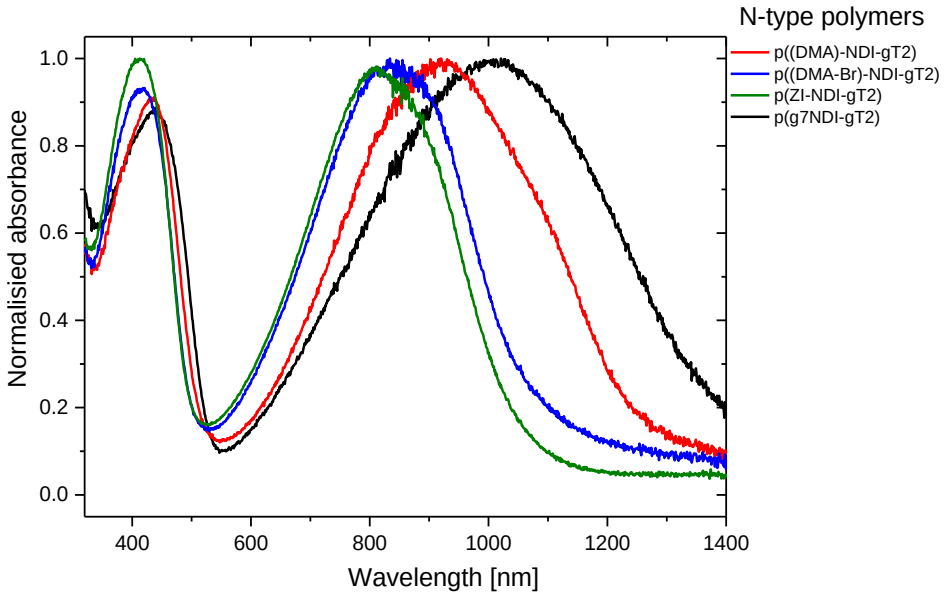


Figure S25. Normalized UV-Vis spectra of the n-type copolymers prepared by spin coating or doctor blade coating on glass substrates.

# 8 Electrochemical and spectroelectrochemical measurements

## 8.1 Sample preparation:

Spectroelectrochemical measurements:

The preparation of samples presented in the main text was carried out according to the following procedure: fluorine doped tin oxide (FTO TEC15) or indium doped tin oxide (ITO) coated glass substrates were cleaned with soap, deionized water acetone and isopropanol before undergoing a heating step at 450°C for 30 minutes. The polymers were dissolved in organic solvents (chloroform for p(gT2) and p(g7NDI-gT2) (5 mg/mL) and DMSO for p(ZI-NDI-gT2) (5 mg/mL)) and deposited from solution onto the substrates via spin coating, drop casting or doctor blading.

p(gT2) and p(g7NDI-gT2) were deposited at room temperature, while for p(ZI-NDI-gT2) the deposition was performed on a hot plate and followed by an additional heating step in order to remove residuals of solvent in the film. Temperatures in the range between 120 and 160°C were used for the deposition and post-processing of the film and yielded similar results in terms of electrochemical characterization. Araldite rapid epoxy glue was added whenever it was needed to minimize exposure of FTO/ITO/Au surface to the electrolyte. The measurement of thin film thickness for the polymers was carried out by calibrating against a reference value of absorbance of a samples with known thickness (thickness was measured by using a Dektak profilometer). The thickness of thin films was calculated from optical absorbance of the samples. Films that were thicker than 200 nm were measured with the profilometer.

Volumetric capacity measurements:

Thick films (>400 nm) were deposited on gold coated glass substrates (with a thin interlayer of parylene to improve adhesion of the gold layer) by either drop casting or blade coating. The area of the devices was defined by removing parts of the polymer and the area was measured with a profilometer. Film thickness was then measuremed by taking the average of at least 6 measurements on each films using a profilometer (in dry-state) before electrochemical characterization. The active area of the samples in this case was in the order of 0.1 $cm^2$.

Drop cast film of p(gT2) on gold substrates with a defined area.

Gravimetric capacity measurements:

For gravimetric measurements of p(gT2), a dilute solution of the polymer was prepared in chloroform (2,2 mg/mL) and 10 µL of this solution was deposited by drop-cast on gold coated substrates (with paryelene interlayer). For p(ZI-NDI-gT2), a solution of 3 mg/mL was prepared and the the solution was deposited whilst heating the substrate to 120 °C, followed by an annealing step at 140 °C for 30 mins.

Drop cast film on gold substrates

## 8.2 Electrochemical measurements in aqueous electrolytes

Electrochemical characterization presented in Figure 4 in the main text was carried out using an Ivium CompactStat potentiostat in an electrochemical cell filled with 0.1 M NaCl aqueous electrolyte (unless stated otherwise), using the polymer film as the working electrode of the cell, a Ag/AgCl 3 M NaCl reference electrode and a platinum-mesh counter electrode (active area 25 x 35 mm). The electrolyte was flushed with argon for at least 15 minutes before the beginning of measurements to avoid faradaic side reactions with molecular oxygen during reduction of the n-type polymers. Galvanostatic measurements were performed by applying a sequence of charging and discharging constant current levels to the sample and monitoring the voltage of the sample (for measurements of single electrodes) or of the cell (for measurements on the two-electrode cell). The charging and the discharging currents were of same magnitude in all cases. Multiple consecutive cycles were performed to evaluate the rate capabilities of the electrodes and of the two-electrode cell for each value of applied current and the $2^{nd}$ cycle was used to calculate the specific capacity illustrated in Figure 5. The value of C rate for each Galvanostatic measurement was calculated on the basis of the set current density and the value of reversible charge density obtained from the measurement using the slowest rate performed on the electrode. Regarding the cyclic voltammetry characterization, the two-electrode cell was scanned to a negative potential (between -0.8 V and -1 V) to reset the neutrality of the p-type polymer between scans presented in Figure 6c. This procedure was followed to avoid distortion in the CV profiles due to charge retention unbalance between the cathode and anode electrodes. This effect and its consequences are discussed in detail in Figure S52.

## 8.3 Spectroelectrochemical measurements in aqueous electrolytes

The electrochemical cell was a quartz cuvette with transparent windows which enabled simultaneous optical spectra acquisition through a UV-vis spectrometer (OceanOptics USB 2000+) which collected the transmitted light through the sample from a tungsten lamp used as probe light source. Spectroelectrochemical measurements on a two-electrode cell including both p-type and an n-type polymer films were performed in a similar way, using a 2 electrode configuration and by monitoring the optical absorption of both films in series.

# 9 Quantum chemical calculations

Spectra Calculations

Molecules in their neural, singly and doubly reduced (for n-type) or oxidized (for p-type) states were optimized at the DFT level (B3LYP/6-31g(d,p)) with water included as a Polarizable Continuum Model (PCM). TD-DFT calculations were then performed on the optimized geometries (B3LYP/6-31g(d,p)) also with water solvent (PCM) to obtain absorption spectra. All quantum chemical calculations were done using Gaussian16.[3]

In order to reproduce experimental data on p(gT2), oligomers $(gT2)_n$ with n=1, 3 and 6 were calculated using above described procedure. For neutral systems, the lowest energy absorption peak position red-shifts with increasing number of monomer units from 337 nm for monomer, 618 nm for trimer to 804 nm for hexamer. These spectra are presented in Figure S26. The experimental value is around 645 nm as shown in the main text. On this basis, we chose the trimer - $(gT2)_3$ as a reference molecule to compare with experimental results (the chemical structure of $(gT2)_3$ is shown in Figure S27). Figure S28 presents calculated spectra of $(gT2)_3$ in its neutral ('0'), singly ('+1') and doubly ('+2') oxidized states with Gaussian broadening equal 0.15 eV. Bottom panel of Figure S28 presents different linear combinations of these three spectra to illustrate some of the expected intermediate states. Table S1 presents calculated active excited states energies and corresponding oscillator strengths of $(gT2)_3$, $(gT2)_3^{+1}$ and $(gT2)_3^{+2}$.

To reduce computational time, n-type polymers p(g7NDI-gT2) and p(ZI-NDI-gT2) were approximated by their monomers with shorter side chains. Figure S29 shows structural formulas of monomers named g1DI-gT2 and ZI-NDI-gT2, both consist of NDI core with ethylene glycol (g1NDI) or zwitterion (ZI-NDI) side chains and methoxy bithiophene (gT2). Figure S30 and S31 show spectra of monomers in their neutral, singly and doubly reduced states with Gaussian broadening equal 0.25 eV. Bottom panels include spectra of partially charged species. Table S2 and S3 consist of list of excited states and corresponding oscillator strengths for g1DI-gT2 and ZI-NDI-gT2 respectively.

Charge distribution calculations

Together with optical spectra, charge distributions across molecules in different oxidation states were calculated using CHEL PG scheme (Charges from Electrostatic Potentials using a Grid-based method) implemented in Gaussian16. In order to simplify n-type polymers are represented by symmetric monomers with shorter side chains in vacuum (gT-g1NDI-gT and gT-ZI-NDI-gT). Molecules are divided into fragments, indicated with different colors in Figure S32 and Figure S33. Table S4 and Table S5 show total charge distributions for these fragments in neutral, polaron and bipolaron states of gT-g1NDI-gT and gT-ZI-NDI-gT respectively. Differences between neutral and polaron states and bipolaron and polaron states are also included in the tables.

As we comment in the main text of the paper, most of the added charge is distributed within the NDI core. In the case of gT-g1NDI-gT, 68% of the first extra electron (polaron) and 67% of the second extra electron (bipolaron) are located on the NDI. In the zwitterion case – gT-ZI-NDI-gT, the addition of the first extra electron causes an even stronger polarization in the side chains than in the neutral molecule and thus stronger charge localization on NDI – 85%. Including a second electron already breaks this trend. Only 58% of its charge is localized on NDI, the rest is spread among side chains and thiophenes.

In both molecules, the oxygen atoms in the NDI group are negatively charged in the neutral state and become even more negative upon reduction, much more than their neighboring positively charged carbons. This fact suggests that oxygens are favored locations for extra electrons in the first and second reductions of gT-g1NDI-gT and gT-ZI-NDI-gT and justifies the reduction mechanism proposed in reference [4].

## 9.1 p(gT2)

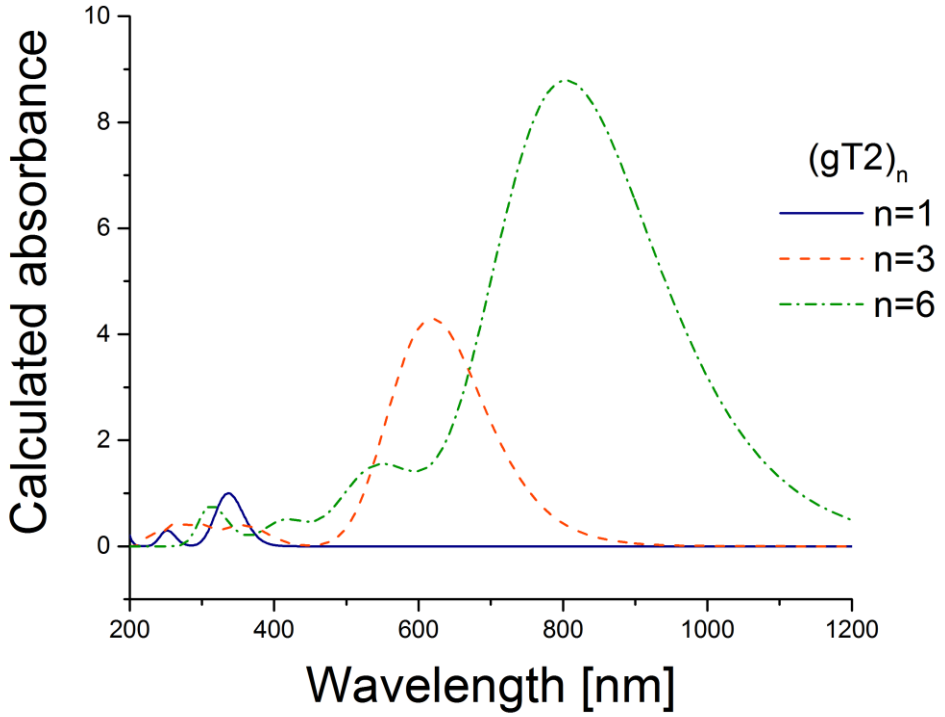


Figure S26. TD-DFT calculated absorption spectra of the monomer, trimer and hexamer $(gT2)_n$ in water(PCM) in their neutral state normalized to the spectra of monomer. In order to reproduce experimental data on p(gT2), oligomers $(gT2)_n$ with n=1, 3 and 6 were calculated using above described procedure. For neutral systems, the lowest energy absorption peak position red-shifts with increasing number of monomer units from 337 nm for monomer, 618 nm for trimer to 804 nm for hexamer. The experimental value is around 645 nm as shown in Table 1 of the main text. On this basis, we chose the trimer - $(gT2)_3$ as a reference molecule to compare with experimental results (the chemical structure of $(gT2)_3$ is shown in Figure S27).

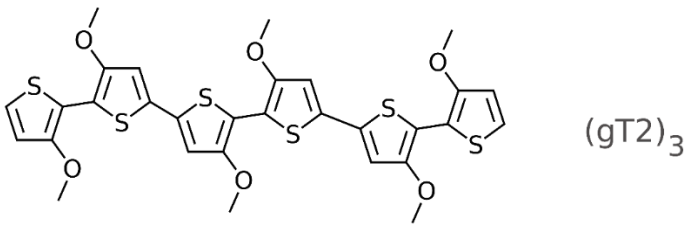


Figure S27. Chemical structure of the trimer $(gT2)_3$.

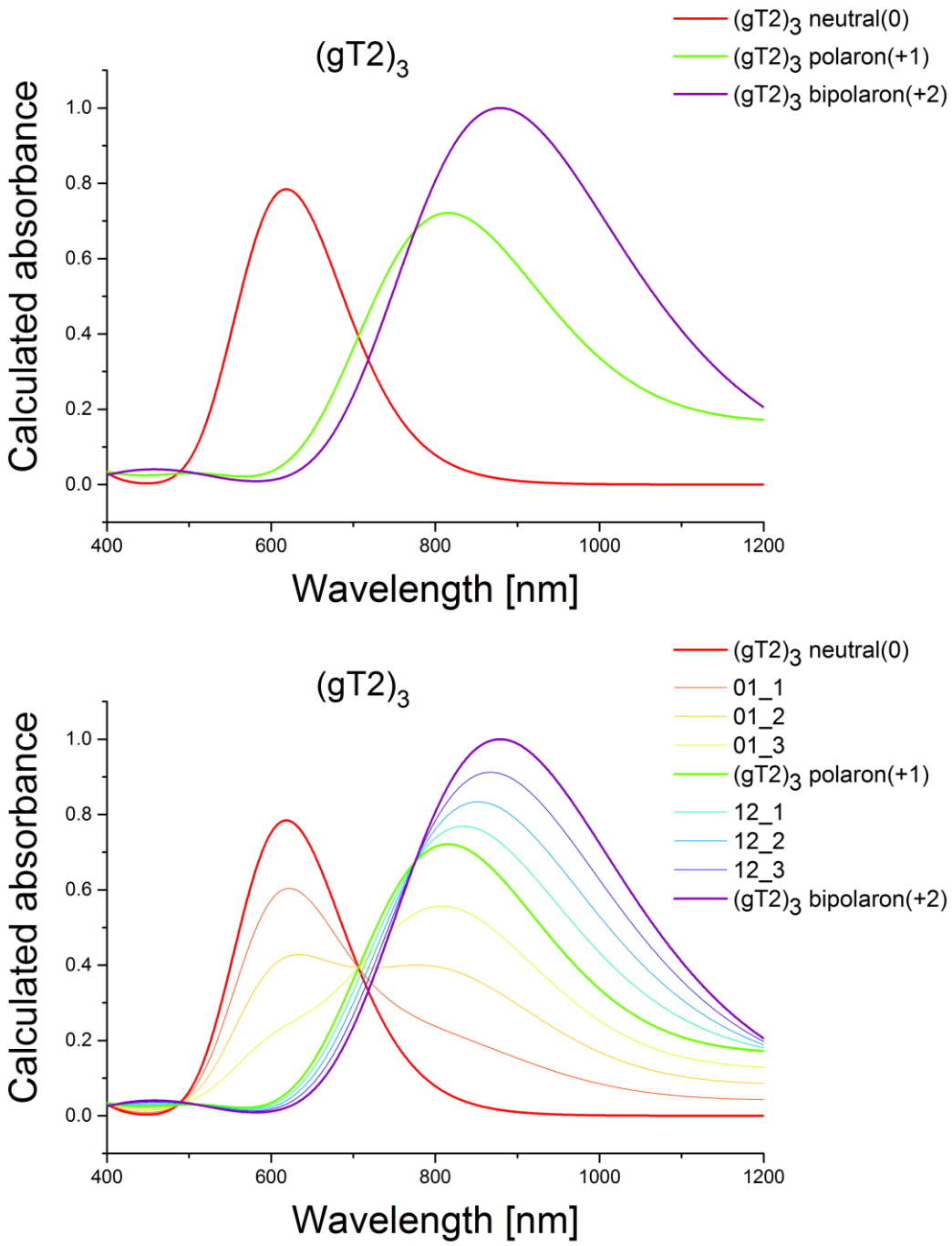


Figure S28. TD-DFT simulated absorption spectra of unchanged and charged state for the p(gT2) polymer in water solution. (top) TD-DFT calculated absorption spectra of the trimer $(gT2)_3$ in water(PCM) in its neutral, singly and doubly oxidized state normalized to the spectra of neutral trimer. (bottom) Linear combination of the spectra qualitatively reproducing results shown in the main text for p(gT2). In the legend eg. '01_2' means the second (2) out of five step between neutral (0) and singly oxidized (1) trimer. Other names were created analogously.

*Table S1. Energies and oscillator strengths calculated for $(gT2)_3$, $(gT2)_3^{+1}$ and $(gT2)_3^{+2}$* in water(PCM) *up to 3.54eV (350nm). The last entry in the columns indicates states in the given energy interval and sum of oscillator strengths of these states.*

| **Neutral $(gT2)_3$** | | **$(gT2)_3^{+1}$** | | **$(gT2)_3^{+2}$** | |
|---|---|---|---|---|---|
| Energy [eV (nm)] | Oscillator strength | Energy [eV (nm)] | Oscillator strength | Energy [eV (nm)] | Oscillator strength |
| 2.00 (618.6) | 2.19 | 0.89 (1388.8) | 0.42 | 1.41 (878.9) | 2.80 |
| 3.13 (395.1) | 0.004 | 1.52 (814.7) | 2.01 | 2.48 (499.0) | 0.05 |
| 3.31 (374.1) | 0.13 | 2.22 (559.8) | 0.002 | 2.54 (488.5) | 0.02 |
| 3.61 (343.0) | 0.13 | 2.37 (521.6) | 0.04 | 2.75 (450.4) | 0.04 |
| | | 2.44 (507.2) | 0.02 | 2.86 (432.6) | 0.03 |
| | | 2.63 (471.7) | 0.02 | 3.03 (409.1) | 0.04 |
| | | 2.78 (445.5) | 0.02 | | |
| | | 2.94(422.1) – -3.41 (363.0) | 0.15 | | |

## 9.2 n-type polymer - p(g7NDI-gT2) and p(ZI-NDI-gT2)

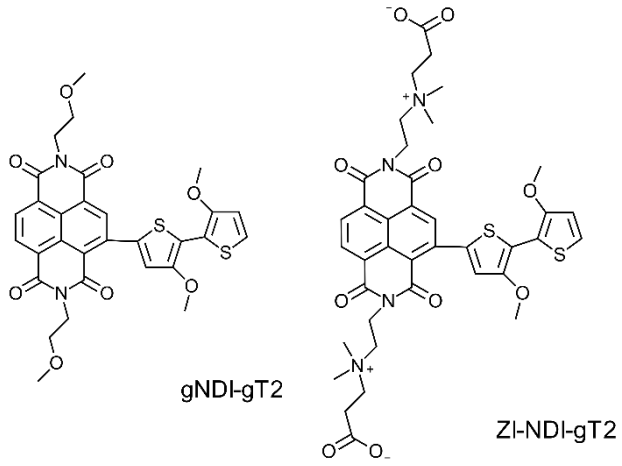


Figure S29. Structural formulas of calculated monomers of g1NDI-gT2 and ZI-NDI-gT2.

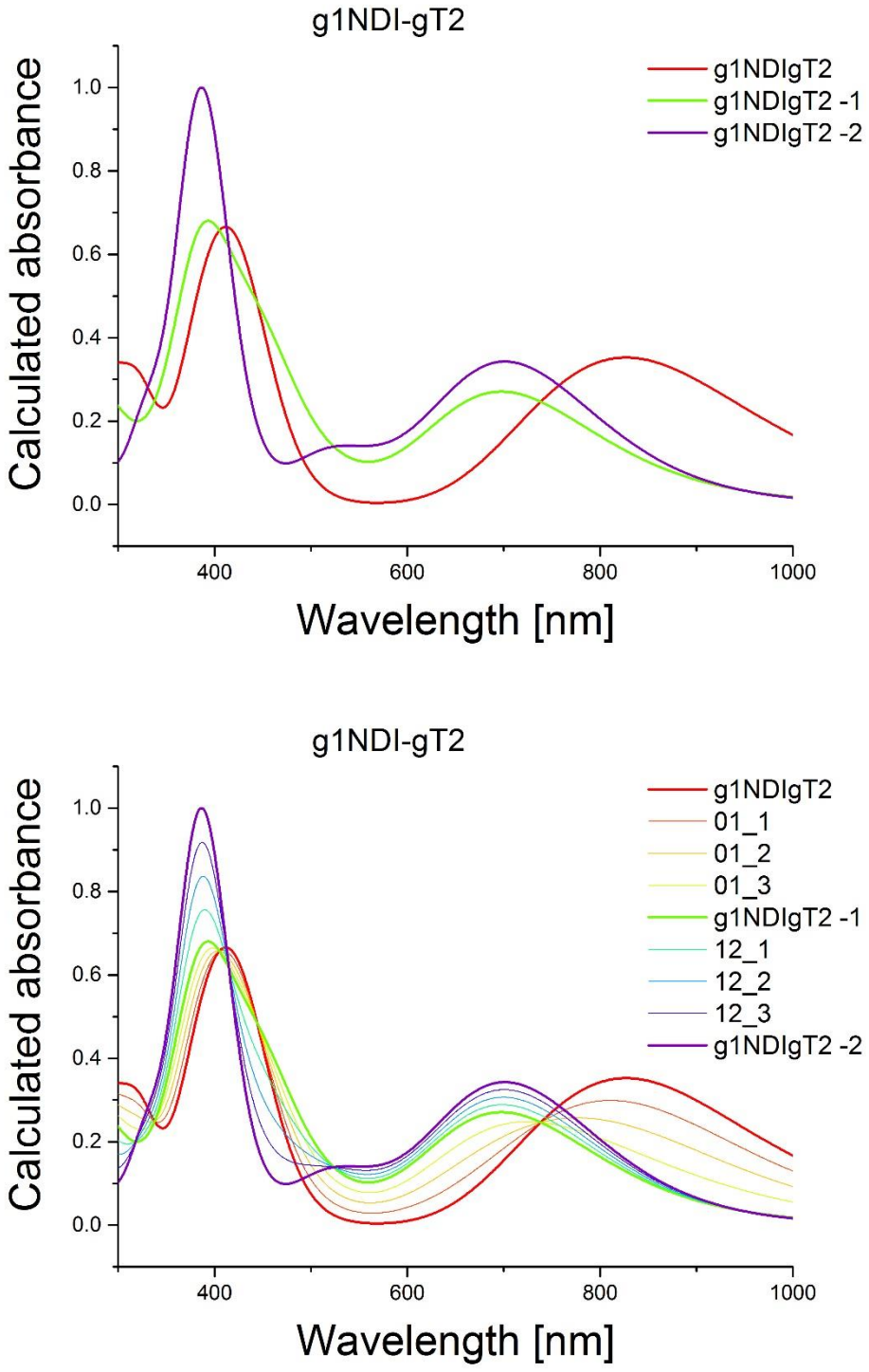


Figure S30. TD-DFT simulated absorption spectra of unchanged and charged state for the p(g7NDI-gT2) polymer in water solution. (top) normalized TD-DFT calculated absorption spectra of the monomer g1NDI-gT2 in its neutral, singly and doubly reduced (bottom) Linear combination of the spectra qualitatively reproducing results shown in Figure S36 for p(g7NDI-gT2). In the legend eg. '01_2' means the second (2) out of three step between neutral (0) and singly reduced (1) molecules. Other names were created analogously.

Table S2. Energies and oscillator strengths calculated for g1NDI-gT2, g1NDI-gT2 $^{-1}$ and g1NDI-gT2 $^{-2}$ in water (PCM) up to 3.54eV (350nm). The last entry in the columns indicates states in the given energy interval and sum of oscillator strengths of these states.

| **Neutral g1NDI-gT2** | | **g1NDI-gT2 $^{-1}$** | | **g1NDI-gT2 $^{-2}$** | |
|---|---|---|---|---|---|
| Energy [eV (nm)] | Oscillator strength | Energy [eV (nm)] | Oscillator strength | Energy [eV (nm)] | Oscillator strength |
| 1.50 (827.1) | 0.35 | 1.57 (787.4) | 0.03 | 1.76 (703.5) | 0.34 |
| 2.70 (459.8) | 0.01 | 1.78 (693.7) | 0.24 | 2.35 (527.6) | 0.13 |
| 2.86 (433.5) | 0.14 | 1.98 (627.7)- -2.34 (529.6) | 0.06 | 2.70 (458.7) | 0.02 |
| 2.91 (425.8) | 0.33 | | | 3.16 (392.5) | 0.38 |
| 3.14 (395.0) | 0.10 | 2.69 (459.7)- -2.87 (432.7) | 0.37 | 3.22 (385.1) | 0.59 |
| 3.21 (386.0) | 0.24 | | | 3.54 (350.3) | 0.06 |
| 3.24 (382.2)- -3.49 ( 355.5) | 0.05 | 3.11 (398.4) | 0.23 | | |
| | | 3.12 (396.4)- -3.48 (355.7) | 0.46 | | |

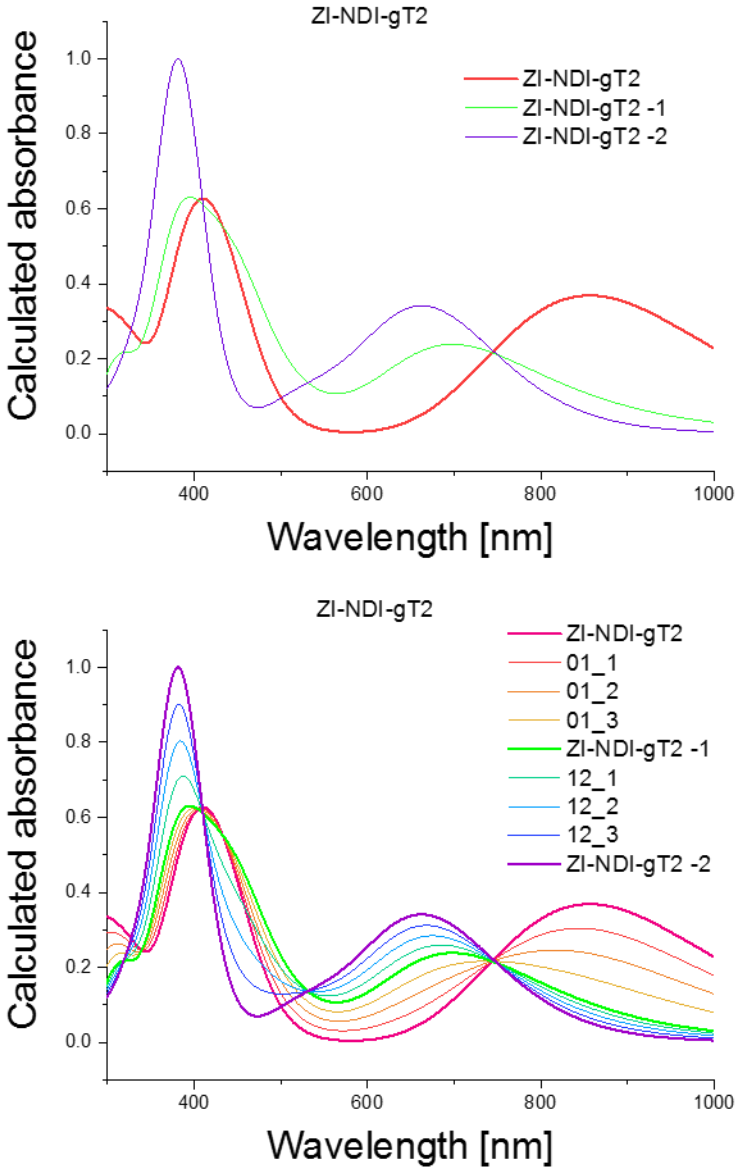


Figure S31. TD-DFT simulated absorption spectra of unchanged and charged state for the p(ZI-NDI-gT2) polymer in water solution (top) normalized TD-DFT calculated absorption spectra of the monomer ZI-NDI-gT2 in its neutral, singly and doubly reduced state (bottom) Linear combination of the spectra qualitatively reproducing results shown in the main text for p(ZI-NDI-gT2). In the legend eg. '01_2' means the second (2) out of three step between neutral (0) and singly reduced (1) molecules. Other names were created analogously.

Table S3. Energies and oscillator strengths calculated for ZI-NDI-gT2, ZI-NDI-gT2$^{-1}$ and ZI-NDI-gT2 $^{-2}$ in water (PCM) up to 3.54eV (350nm). The last entry in the columns indicates states in the given energy interval and sum of oscillator strengths of these states.

| **Neutral ZI-NDI-gT2** | | **ZI-NDI-gT2 $^{-1}$** | | **ZI-NDI-gT2 $^{-2}$** | |
|---|---|---|---|---|---|
| Energy [eV (nm)] | Oscillator strength | Energy [eV (nm)] | Oscillator strength | Energy [eV (nm)] | Oscillator strength |
| 1.45 (856.1) | 0.37 | 1.52 (817.8) | 0.055 | 1.86 (668.0) | 0.35 |
| 2.63 (471.6) | 0.01 | 1.80 (690.0) | 0.21 | 2.32 (533.8) | 0.01 |
| 2.78 (446.0) | 0.07 | 1.98 (627.8) | 0.011 | 2.75 (451.6) | 0.16 |
| 2.85 (433.8) | 0.30 | 2.22 (559.3) | 0.0018 | 3.18 (389.6) | 0.45 |
| 3.06 (405.4) | 0.14 | 2.35 (527.2) | 0.064 | | |
| 3.19 (388.7) | 0.28 | 2.71 (457.5) – 2.73 (454.3) | 0.25 | 3.27 (379.3) | 0.52 |
| 3.29 (376.5)- - 3.52 (352.2) | 0.07 | 2.79 (443.9) | 0.023 | 3.57 (347.3) – 3.91 (316.9) | 0.32 |
| | | 2.86 (433.2) | 0.13 | | |
| | | 3.03 (408.8) | 0.11 | | |
| | | 3.13 (396.4) | 0.16 | | |
| | | 3.16 (392.1) | 0.005 | | |
| | | 3.21 (386.1) | 0.12 | | |
| | | 3.26 (380.4) | 0.030 | | |
| | | 3.31 (374.7) | 0.073 | | |
| | | 3.38 (367.2) – 3.55 (348.9) | 0.179 | | |
| | | 3.71(333.4) – 4.13 (300.0) | 0.240 | | |

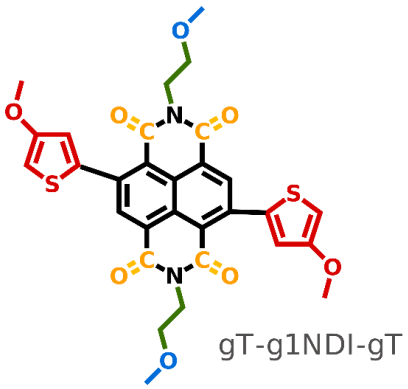


Figure S32. Molecules' sections of gT-g1NDI-gT proposed to clarify charge distribution presented in Table S4.

Table S4. Calculated charge distribution on selected fragments of gT-g1NDI-gT (colored in Figure S32). The values related to the neutral, polaron and bipolaron states are shown in columns 2, 3 and 5. Columns 4 and 6 consist of differential charge, being the difference in charge distribution between neutral and polaron states and bipolaron and polaron states respectively.

| **Molecule's fragment** | **gT-g1NDI-gT Neutral** | **gT-g1NDI-gT Polaron -1** | Charge difference between | **gT-g1NDI-gT Bipolaron -2** | Charge difference between |
|---|---|---|---|---|---|

| | | | | **polaron** and **neutral state** | | **bipolaron** and **polaron state** |
|---|---|---|---|---|---|---|
| $(CH_2O)_2$ | | -0.4 | -0.47 | -0.07 | -0.55 | -0.07 |
| $(C_2H_4)_2$ | | +0.73 | +0.74 | -0.01 | +0.73 | -0.00 |
| C=O | $C_4$ | +2.32 | +2.27 | -0.09 | +2.07 | -0.16 |
| | $O_4$ | -1.77 | -1.99 | -0.22 | -2.22 | -0.23 |
| NDI (without C=O) | | -0.84 | -1.21 | -0.37 | -1.49 | -0.28 |
| $(gT)_2$ | | -0.03 | -0.29 | -0.25 | -0.54 | -0.25 |

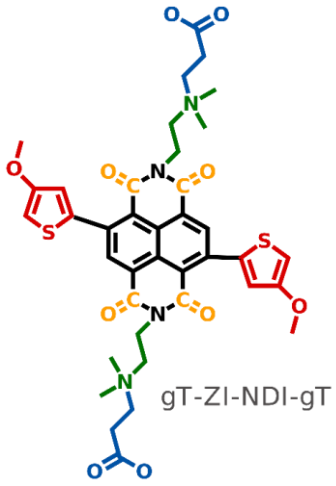


Figure S33. Molecules' sections of gT-ZI-NDI-gT proposed to clarify charge distribution presented in Table S5.

*Table S5. Calculated charge distribution on selected fragments of gT-ZI-NDI-gT (colored in Figure S33). The values related to the neutral, polaron and bipolaron states are shown in columns 2, 3 and 5. Columns 4 and 6 consist of differential charge that is the difference in charge distribution between neutral and polaron states and bipolaron and polaron states respectively.*

| **Molecule's fragment** | | **gT-ZI-NDI-gT Neutral** | **gT-ZI-NDI-gT Polaron -1** | Charge difference between **polaron** and **neutral state** | **gT-ZI-NDI-gT Bipolaron -2** | Charge difference between **bipolaron** and **polaron state** |
|---|---|---|---|---|---|---|
| $(C_3H_4O_2)_2$ | | -1.13 | -1.34 | -0.21 | -1.44 | -0.1 |
| $(C_4H_{10}N)_2$ | | +1.51 | +1.67 | +0.16 | +1.52 | -0.15 |
| C=O | $C_4$ | +2.52 | +2.45 | -0.18 | +2.08 | -0.37 |
| | $O_4$ | -1.89 | -2.1 | -0.21 | -2.27 | -0.17 |
| NDI (without C=O) | | -0.98 | -1.44 | -0.46 | -1.48 | -0.04 |
| $(gT)_2$ | | -0.02 | -0.23 | -0.21 | -0.41 | -0.17 |

# 10 Further electrochemical investigation and stability of p(gT2), p(ZI-NDI-gT2) and p(7NDI-gT2)

## 10.1 p(gT2)

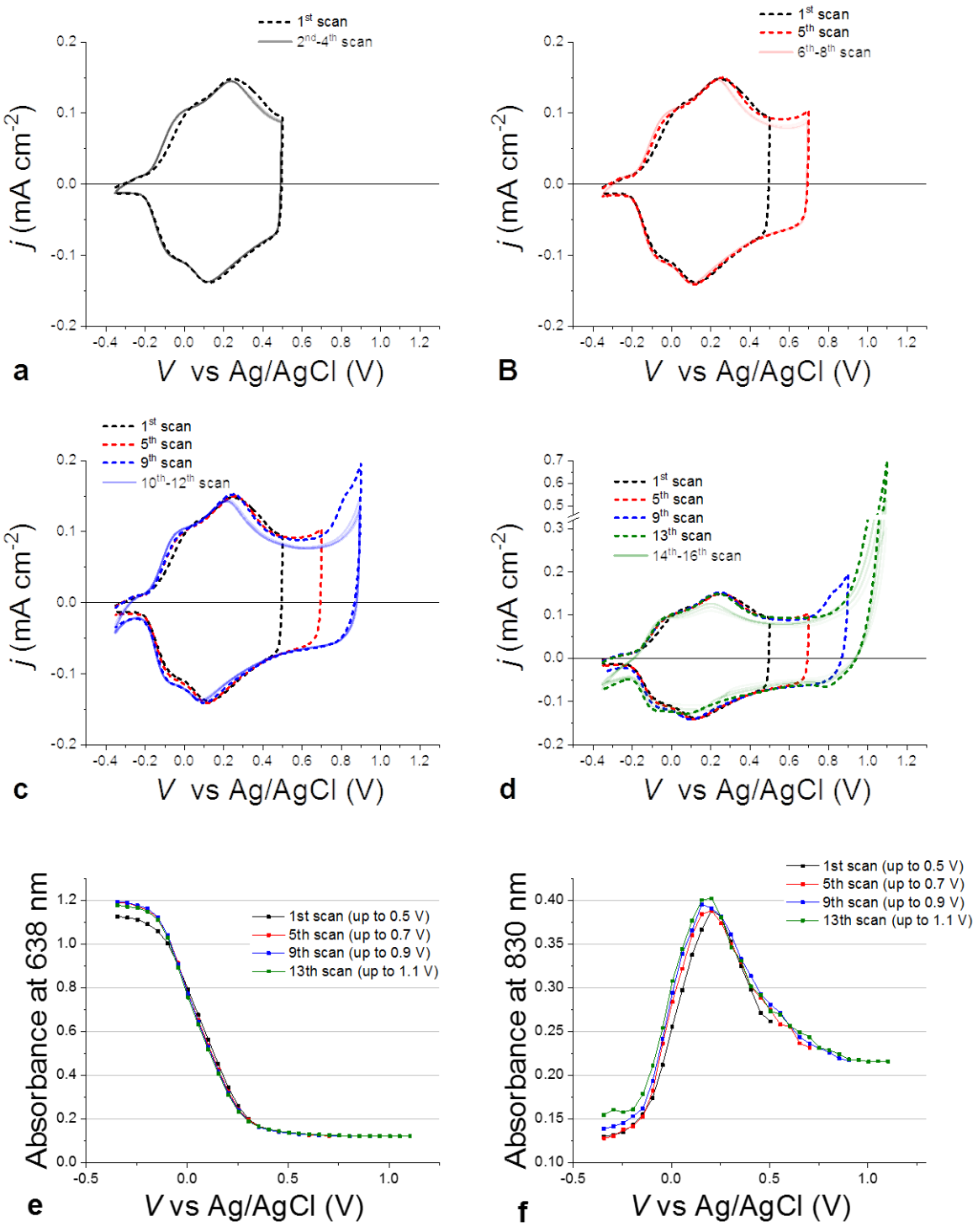


Figure S34. Electrochemical charging and reversibility of p(gT2) on FTO glass. (a) to (d) consecutive cyclic voltammetry measurements performed on a p(gT2) polymer film deposited on FTO in 0.1 M NaCl:DIW at scan rate of 50 mV $s^{-1}$. Absorbance evolution monitored at (e) 638 nm and (f) 830 nm as a function of applied voltage during the CV scans shown in (a)-(d). The formation of bipolarons in the

film, which can be monitored as the drop in absorbance at 830 nm after the first peak in (f), appears to complete at voltages of about 1.1 V.

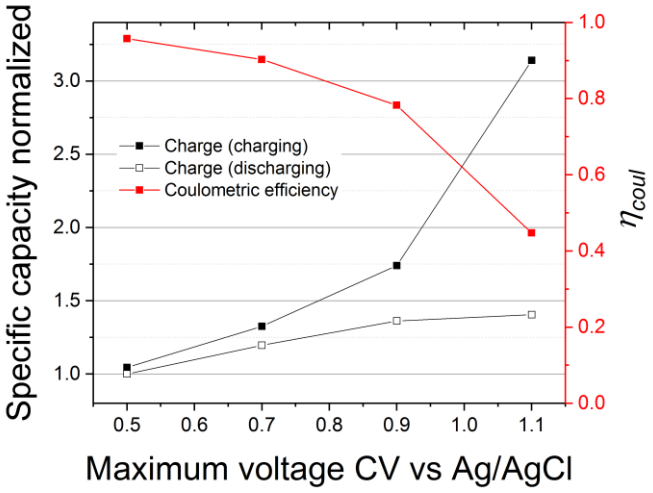


Figure S35. Specific capacity and coulombic efficiency of a p(gT2) film scanned up to different maximum potential vs Ag/AgCl of a cyclic voltammetry measurement.

## 10.2 p(g7NDI-gT2)

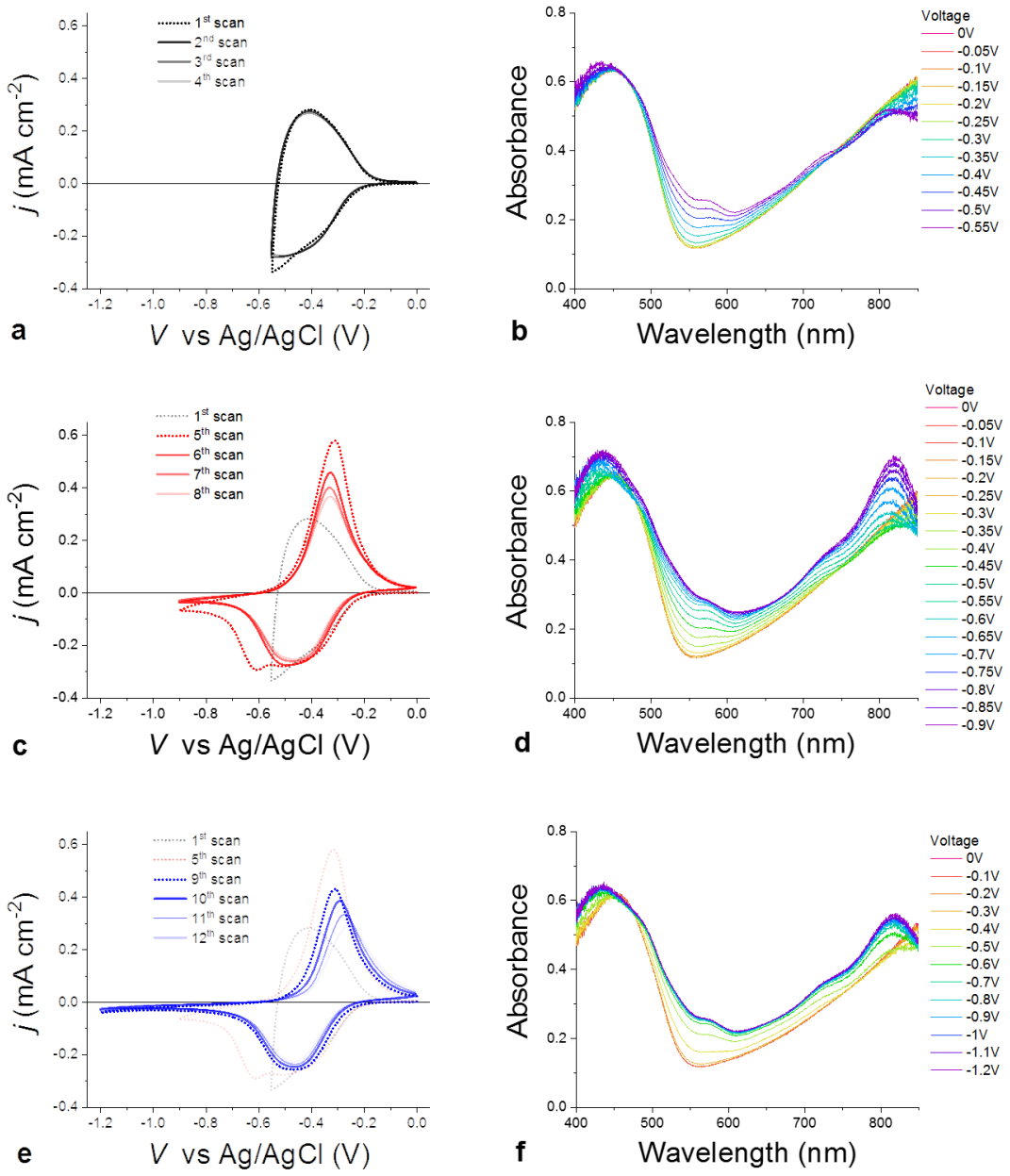


Figure S36. Reversibility and electrochemical charging of p(g7NDI-gT2) n-type polymer. (a), (c), (e) consecutive cyclic voltammetry measurements performed on a p(g7NDI-gT2) polymer film deposited on FTO in 0.1 M NaCl at scan rate of 50 mV $s^{-1}$ reaching a negative potential of (a) -0.55 V, (c) -0.9 V, (e) -1.2 V vs Ag/AgCl. Film absorbance evolution referred to the (b) 1st, (d) 5th and (f) 9th scan. The presence of a second peak when scanning to potential more negative than -0.55 V vs Ag/AgCl is shown in (c). This peak is not there in the following scans as discussed in the main text. Also, the changes in absorbance detected for the first measurement scanning down to -0.9 V vs Ag/AgCl (5th scan in (c)) are greater than the ones appearing over the following cycles. This suggests that the ability of the film to reversibly reach deep level of charging changes after the first scan to potentials more negative than -0.55 V vs Ag/AgCl. The spectral signatures that we observe at potentials more negative than about -0.4 V vs Ag/AgCl could be ascribed to bipolaron bands.

## 10.3 Stability of p(gT2), p(ZI-NDI-gT2) and p(g7NDI-gT2)

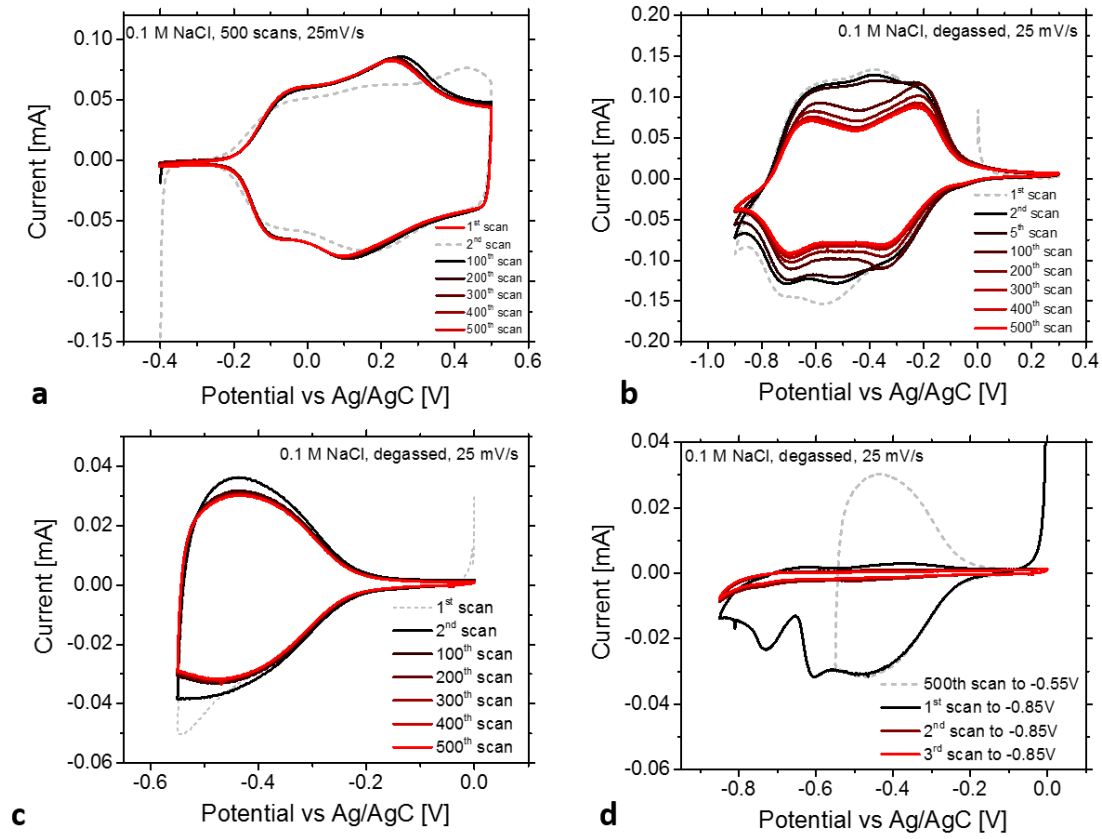


Figure S37. a) Stability measurements (500 scans) of p(gT2), b) p(ZI-NDI-gT2) , c) p(g7NDI-gT2) (-0.55V) and d) p(g7NDI-gT2) (-0.85V) on gold coated glass subtrates in 0.1 M NaCl with a scan rate of 25 mV $s^{-1}$ with a Ag/AgCl as the reference electrode. Degassed electrolytes were used for the n-type. The polymer p(g7NDI-gT2) is delimainting when charging to -0.85 V (the polymer film is the same as the one used to measure stability to -0.55 V).

## 10.4 Gravimetric capacity

The gravimetric capacities of p(gT2), p(ZI-NDI-gT2) and p(g7NDI-gT2) were measured by preparing solutions with known concentrations and the indicated volume of this solutions was drop cast on a gold substarte with a thin parylene interlayer to improve gold adhesion. For p(ZI-NDI-gT2), the substrate was heated to 80 °C during processing of the polymer, followed by a drying step at 140 °C for 30 mins. The accuracy of this method to estimate the gravimetric capacity of the polymers relies on the use of fully dissolved solutions. It is also limited by the accuracy of weighing small amount of polymer, and errors related to dispensing the solution on the conductive substrate. We note that, particularly for p(ZI-NDI-gT2), solubility was limited at the chosen concentration and we expect the values of gravimetric capacity to be underestimated.

p(gT2): 10 µL of a solution (2.2 mg/mL) was drop cast on Au coated glass substartes.

p(ZI-NDI-gT2): 10 µL of a solution (3.75 mg/mL) was drop cast on Au coated glass substartes.

p(g7NDI-gT2): 10 µL of a solution (2.00 mg/mL) was drop cast on Au coated glass substartes.

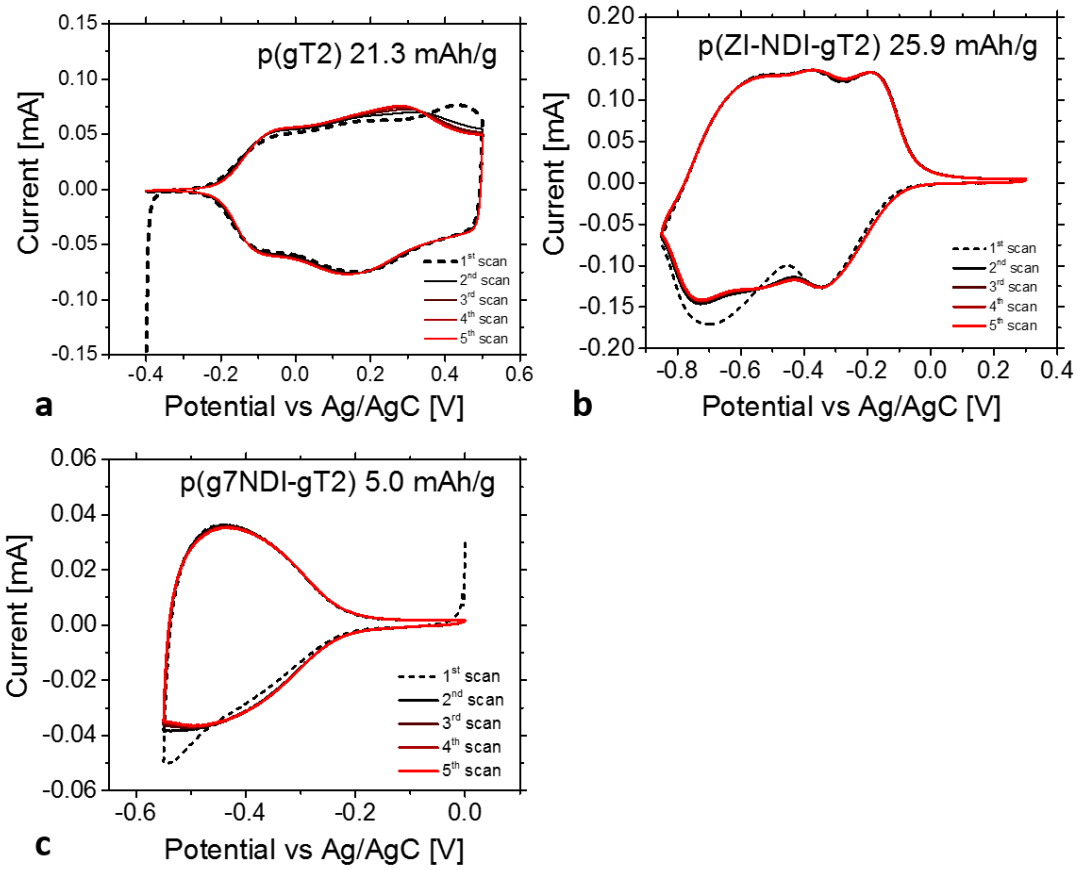


Figure S38. CV measurements of the prepared drop cast devices a) p(gT2) and b) p(ZI-NDI-gT2) and c) p(g7NDI-gT2) in degassed 0.1 M NaCl solution with a scan rate of 25 mV/s.

# 11 Charge density as a function of film thickness for the p-type and n-type polymers.

The thickness dependent charge density of the three polymers were extracted from cyclic voltammetry performed at 50 mV $s^{-1}$. The dotted lines are linear fits with slope 1 on a log-log scale to the data. For the p(gT2) and the p(g7NDI-gT2) polymers, the reversible charge of the second CV was taken for their respective datasets. For p(ZI-NDI-gT2), films deposited from methanol were used for this analysis. The reversible charge from the 1st CV was considered, probably representing an underestimate of the total charge that can be accumulated in films deposited from DMSO (the latter showed higher reversibility). The three datasets show a close to linear relation between charge density and thickness in the range 10 to 200 nm (the fits are run with slope constraint to 1), suggesting that charging and discharging occurs for all the polymers in the second timescale. The resulting specific capacities are shown in the legend.

These values are conservative estimates of the specific capacity for the polymers for the following reasons: (i) For the p(gT2) polymer a value of 25 mAh $cm^{-3}$ was found considering scanning of the polymer up to 0.5 V vs Ag/AgCl. Based on Figure S34 we can conclude that this is an underestimate of the potential specific capacity of p(gT2) polymer films in that larger values are expected when scanning to more positive potentials (up to 35 mAh $cm^{-3}$ when scanning up to 1.1 V vs Ag/AgCl). One expects however the coulombic efficiency to drop significantly under these conditions. (ii) For p(g7NDI-gT2) we consider only the charge accumulated in films scanned to -0.55V vs Ag/AgCl. (iii) For p(ZI-NDI-gT2), films deposited from methanol showed lower reversibility during the first CV scan compared to those deposited from DMSO. The theoretical capacity for the p(gT2) and the p(ZI-NDI-gT2) polymers can be calculated from the volume density of their individual redox-sites and the number of charges that each site can accommodate. Given the extended conjugation of these materials, the exact size of their redox sites is unknown. However, our experimental and computational results suggest that each monomer of the p(ZI-NDI-gT2) can theoretically be charged with two electrons yielding a theoretical capacity of about 51 mAh $cm^{-3}$. The value of 37 mAh $cm^{-3}$ that we observe is then about 70% of the material's theoretical capacity. For p(gT2), the value of 25 mAh $cm^{-3}$ that we measure corresponds to 0.6 holes per monomer unit. We expect that the polymer's individual redox sites involve more than one monomer. For example, if the polaron and bipolaron were to be delocalized on 2 or 3 monomer units, our result would suggest that a theoretical capacity of about 42 mAh $cm^{-3}$ or 28 mAh $cm^{-3}$ can be reached with this polymer. Note that these calculations have assumed a density of 1 g $cm^{-3}$ for the polymers.

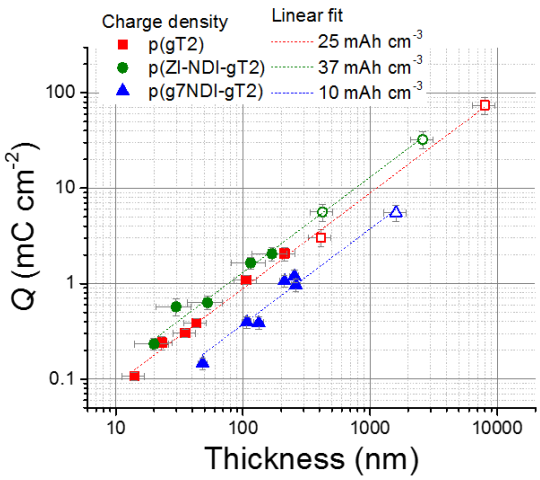


Figure S39. Charge density as a function of film thickness for the p-type and n-type polymers. The full data refer to the reversible capacities measured with cyclic voltammetry at 50 mV $s^{-1}$. The

empty data points refer to the reversible capacity of thicker films measured at the slowest C-rate (between 6 C and 60 C depending on the sample) also shown in Figure 5 of the main text. The linear fit was run with a fixed slope of 1 (on log-log scale) and the value of capacity was calculated from the intercept Y as Capacity(mAh $cm^{-3}$) = $10^{Y}$ $10^{7}/3600$, where the factor $10^{7}/3600$ is used to convert $cm^{-2}$ $nm^{-1}$ to $cm^{-3}$ and from mC to mAh.

# 12 Rate-capabilities of the p-type and n type polymers

## 12.1 p(gT2)

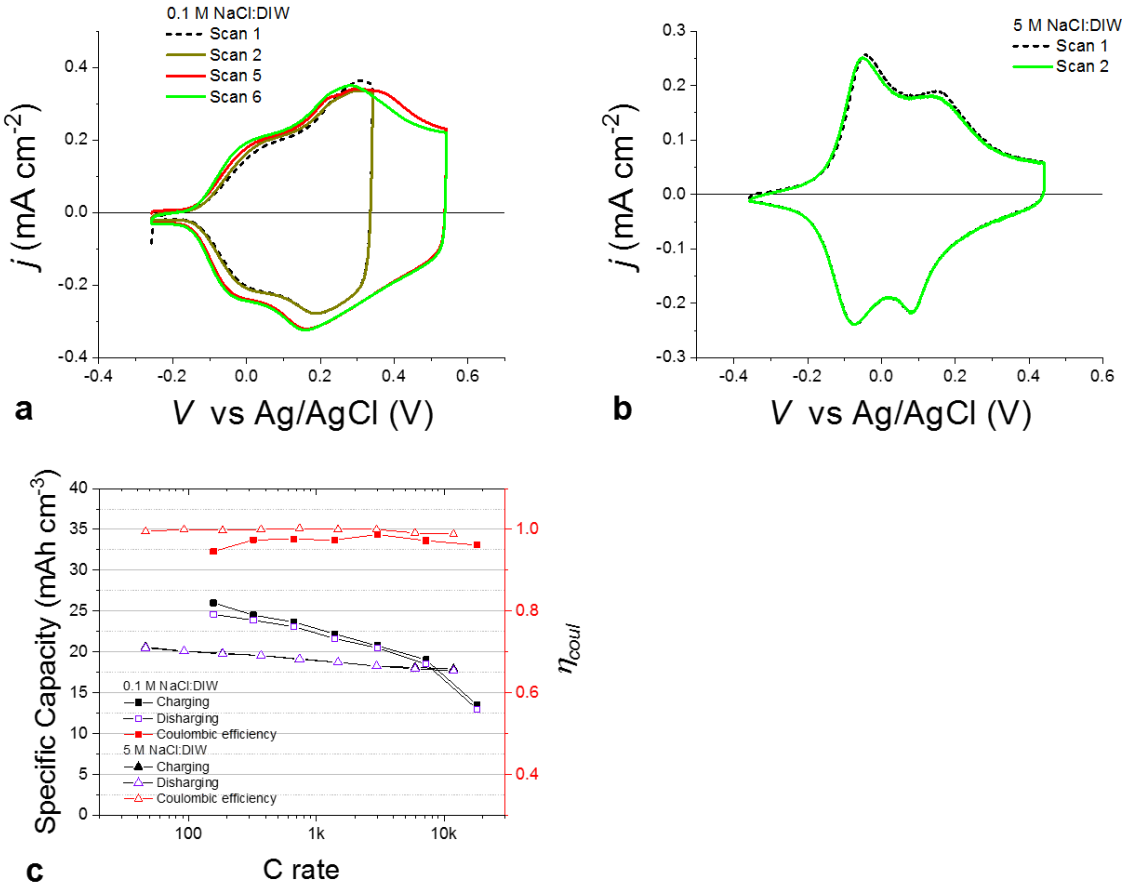


Figure S40. Cyclic voltammetry and Galvanostatic characterization for a p(gT2) polymer film. a)-b) Cyclic voltammetry performed at 50 mV $s^{-1}$ and c) Galvanostatic charging/discharging characterization of a 412 nm p(gT2) film deposited on gold coated glass. Characterization in aqueous 0.1 M NaCl was followed by rinsing of the film in DIW and characterization in aqueous 5 M NaCl. The fractional error associated to the value of specific capacity due to uncertainty in the measurement of the film volume is 22%.

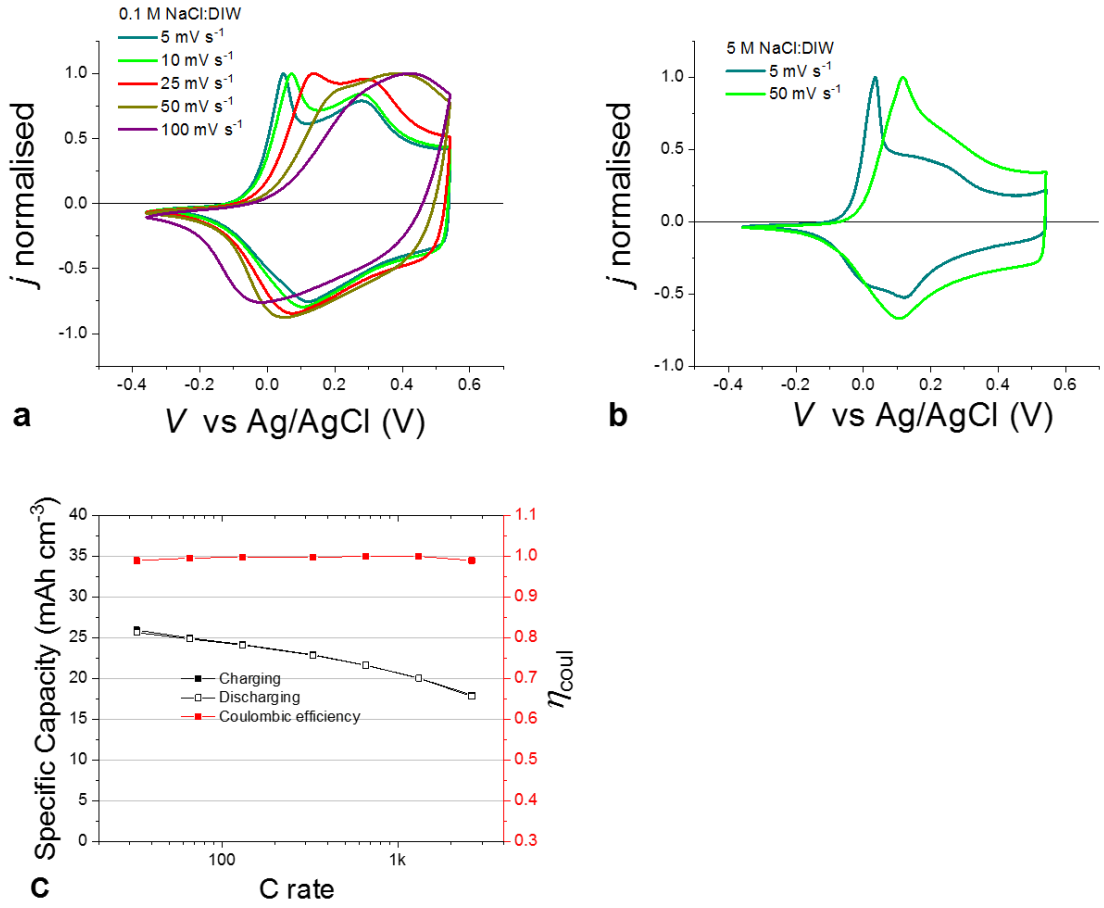


Figure S41. Cyclic voltammetry and Galvanostatic characterization for a p(gT2) polymer thick film. a)-b) Cyclic voltammetry and c) Galvanostatic charging/discharging characterization of a 8 µm p(gT2) film deposited on gold coated glass. Characterization in aqueous 0.1 M NaCl was followed by rinsing of the film in DIW and characterization in aqueous 5 M NaCl. Scan rate dependence of cyclic voltammetry in a) 0.1 M NaCl and b) 5 M NaCl DIW electrolytes. c) shows the rate capabilities of the film in 5 M NaCl aqeuous solution. The fractional error associated to the value of specific capacity due to uncertainty in the measurement of the film volume is 16%.

## 12.2 p(ZI-NDI-gT2)

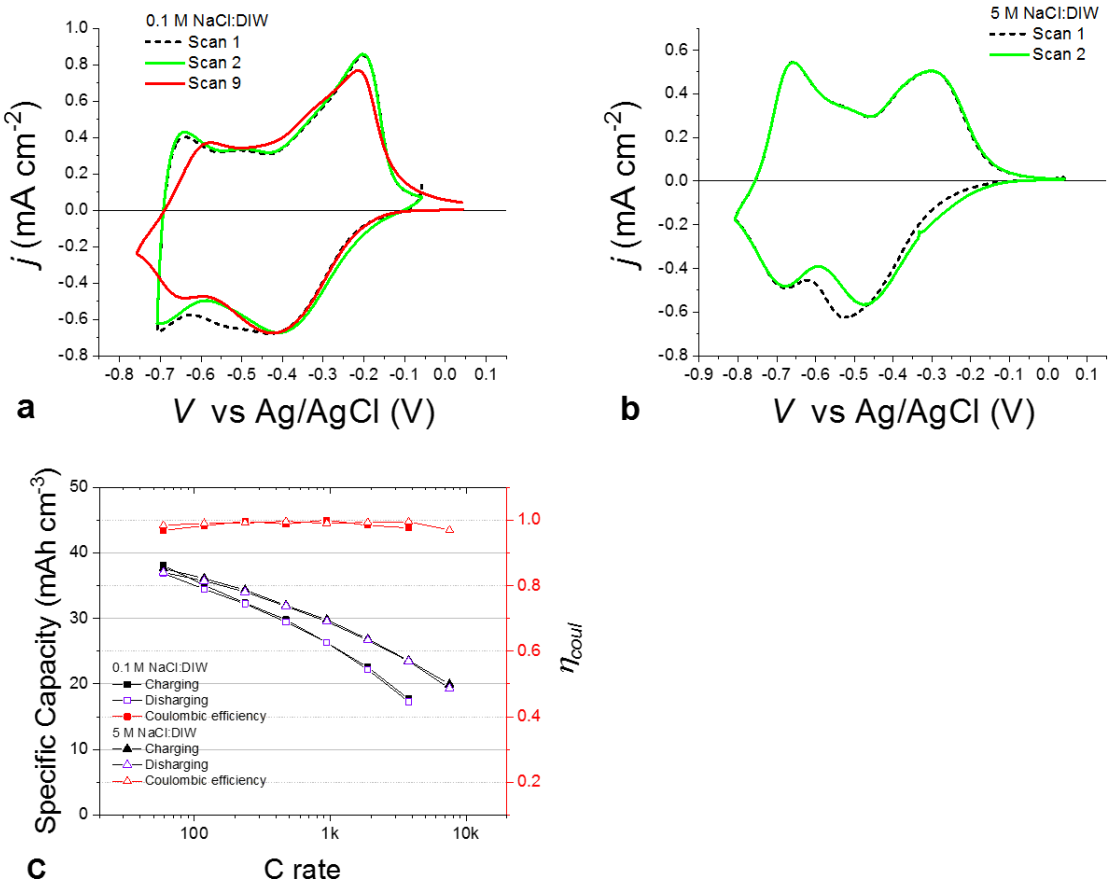


Figure S42. Cyclic voltammetry and Galvanostatic characterization for a p(ZI-NDI-gT2) polymer film. a)-b) Cyclic voltammetry performed at 50 mV $s^{-1}$ and c) Galvanostatic charging/discharging characterization of a 422 nm p(ZI-NDI-gT2) film deposited on gold coated glass. Characterization in aqueous 0.1 M NaCl was followed by rinsing of the film in DIW and characterization in aqueous 5 M NaCl. The fractional error associated to the value of specific capacity due to uncertainty in the measurement of the film volume is 20%.

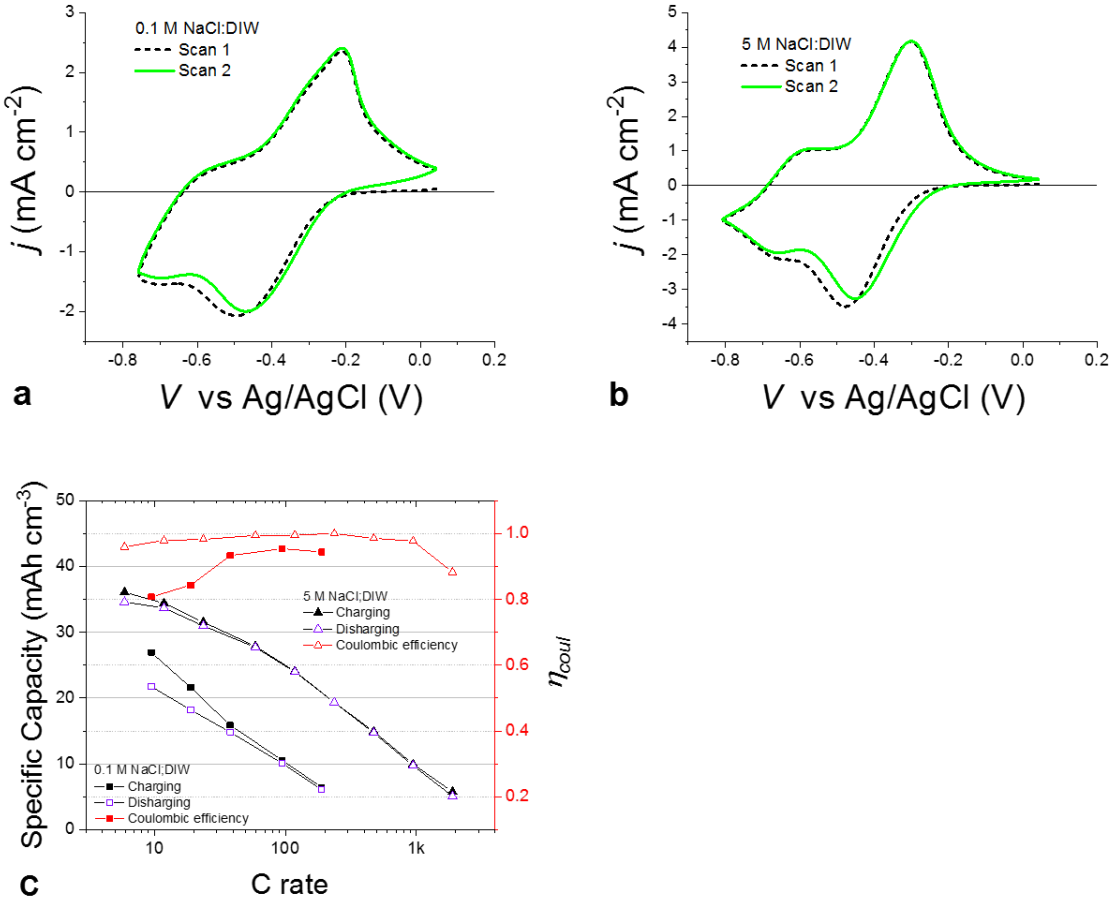


Figure S43. Cyclic voltammetry and Galvanostatic characterization for a p(ZI-NDI-gT2) polymer thick film. a)-b) Cyclic voltammetry performed at 50 mV $s^{-1}$ and (c) Galvanostatic charging/discharging characterization of a 2.6 µm p(ZI-NDI-gT2) film deposited on gold coated glass. Characterization in aqueous 0.1 M NaCl was followed by rinsing of the film in DIW and characterization in aqueous 5 M NaCl. The fractional error associated to the value of specific capacity due to uncertainty in the measurement of the film volume is 21%.

## 12.3 **p(g7-NDI-gT2)**

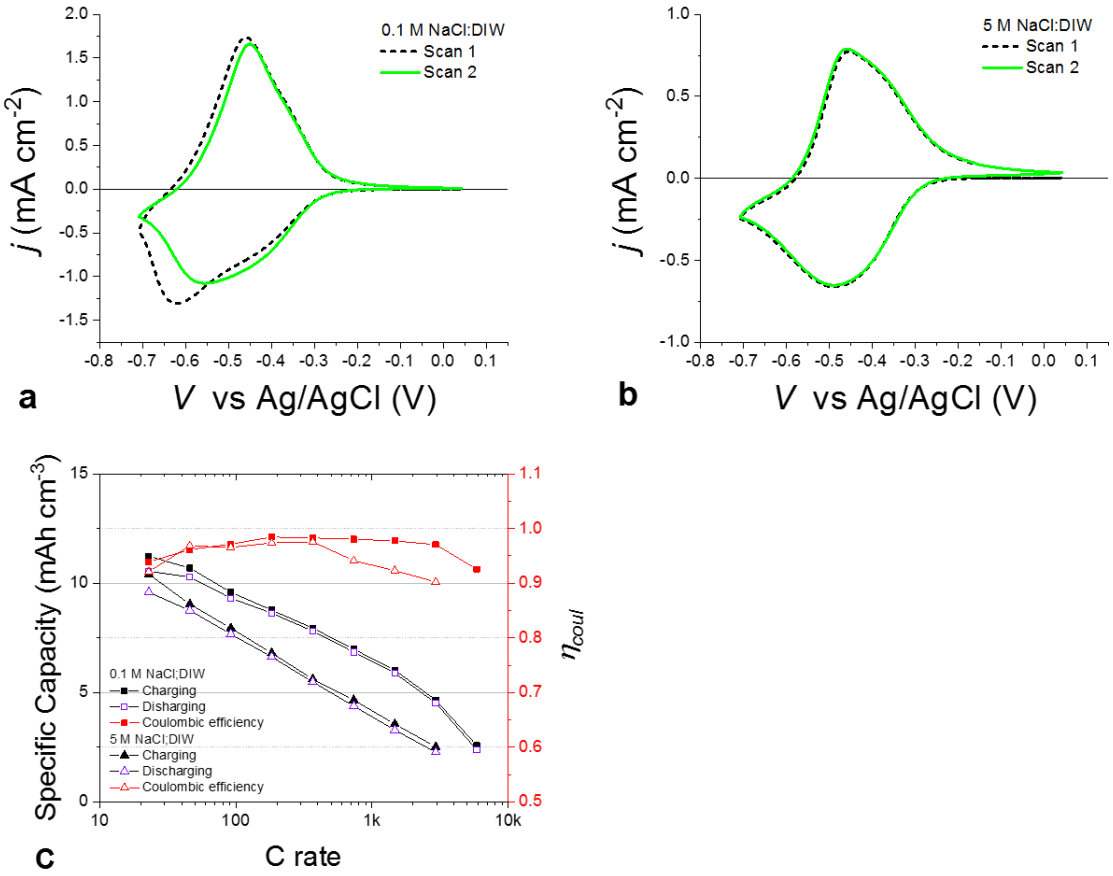


Figure S44. Thick film characterization for p(g7NDI-gT2) polymer. a)-b) Cyclic voltammetry performed at 50 mV $s^{-1}$ and c) Galvanostatic charging/discharging characterization of a 1.6 µm p(g7NDI-gT2) film deposited on gold coated glass. Characterization in aqueous 0.1 M NaCl was followed by rinsing of the film in DIW and characterization in aqueous 5 M NaCl. The fractional error associated to the value of specific capacity due to uncertainty in the measurement of the film volume is 21%.

# 13 Electrochemical cell

## 13.1 Voltage of the electrochemical cell

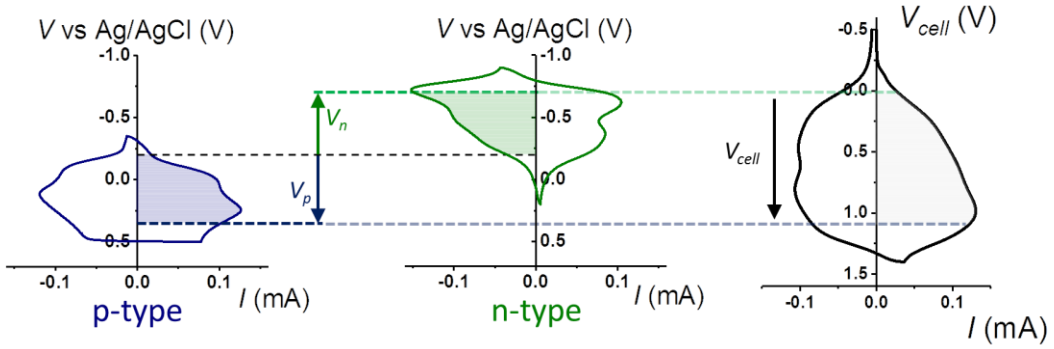


Figure S45. Energetics and charge distribution in the p- and n-type polymers measured in a two-electrode configuratrion: (left and center) cyclic voltammetry measurements on the p-type and the n-type polymers in a three electrode cell at 50 mV $s^{-1}$ (potentials are referenced to Ag/AgCl) and (right) cyclic voltammetry measurement on the complete battery at a scan rate of 100 mV $s^{-1}$. The value $V_{cell}$ is the difference in electrochemical potentials between the p-type (cathode) and n-type (anode) polymers.

## 13.2 Electrochemical response of the two terminal electrochemical cell using films with different thicknesses

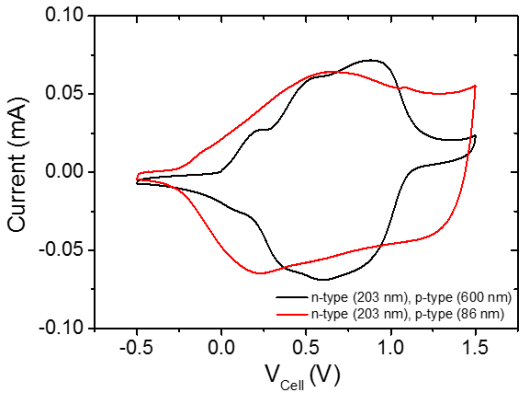


Figure S46. Influence of the p(gT2) film thickness on the electrochemical response of the two electrode cell measured with cyclic voltammetry.

## 13.3 Charge retention

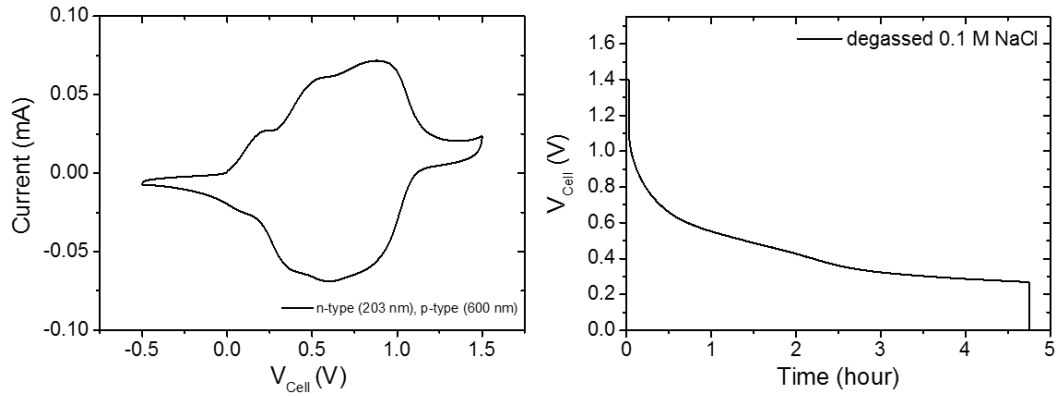


Figure S47. (a) CV of the electrochemical cell before the retention experiment. (b) Retention experiment where a voltage of 1.4 V is applied for 100 s to charge the cell followed by monitoring the potential for 286 min at open circuit. A degassed 0.1 M NaCl solution is used as the supporting electrolyte.

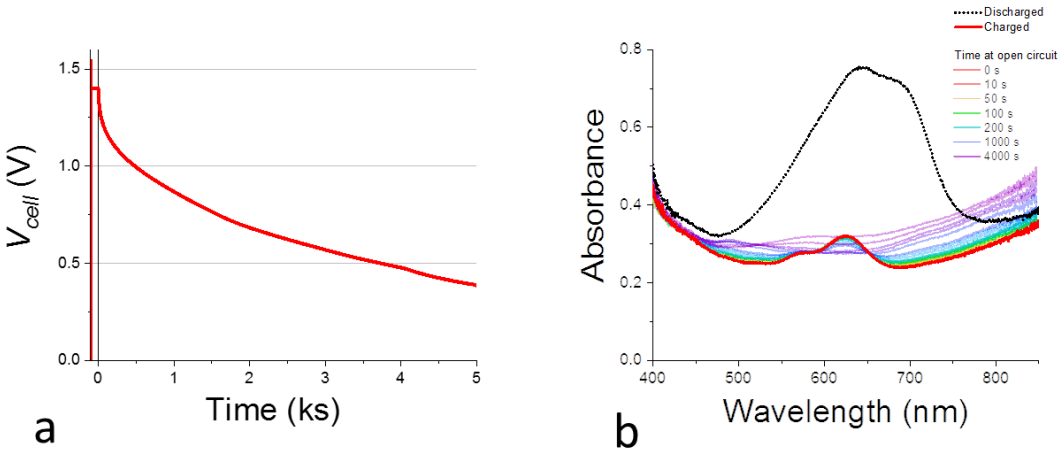


Figure S48. Charge retention experiment performed on the (p(gT2) / 0.1 M NaCl:DIW / p(ZI-NDI-gT2)) two terminal cell shown in the main text. (a) Voltage of the cell as a function of time: the voltage of the device was first kept at 1.4 V for 100 s (Time < 0 s); at Time = 0 s the device was switched to open circuit and its voltage was measured. (b) Optical absorbance of the two polymer films in series as a function of time during the retention measurement.

## 13.4 Hydrogen and oxygen detection

Thin films of p(gT2) and p(ZI-NDI-gT2) on ITO coated glass substrates were prepared and immersed in a 0.1 M degassed NaCl aqeuous solution. $H_2$ and $O_2$ were simultaneously detected in the electrolyte using two Clark electrodes ($H_2$-NP Unisense microsensor for hydrogen, OX-NP Unisense microsensor for oxygen, $O_2$ calibration for 0.1 M NaCl in $H_2O$ at 23 °C).[5] The electrolyte solution was purged with argon prior to the measurement until both electrodes showed a stable voltage output. An argon flow was then maintained in the gas phase of the cell for the first 2.82 h of the measurement in order to prevent oxygen from leaking back into the cell. The oxygen sensor was calibrated against argon-saturated and air-saturated electrolyte.

After stabilisation of the Clark electrode voltage output, the electrochemical cell was charged to 1.4 V for 31 min during which no hydrogen and oxygen evolution was detected (Figure S49a). In addition, no evidence of hydrogen and oxygen formation was observed when charging the cell for additonal 106 min after a 29 min period of no applied potential. After stopping the argon flow in the gas phase, the chronoamperometric current increased immediately, indicating that oxygen rapidy diffuses into the cell and reacts. Despite this current increase, a significant change of the oxygen concentration was only detected with a delay of 13 min after stopping the argon flow, which suggests that small initial amounts of oxygen are converted efficiently. As shown in section 13.5, hydrogen peroxide is a reaction product.

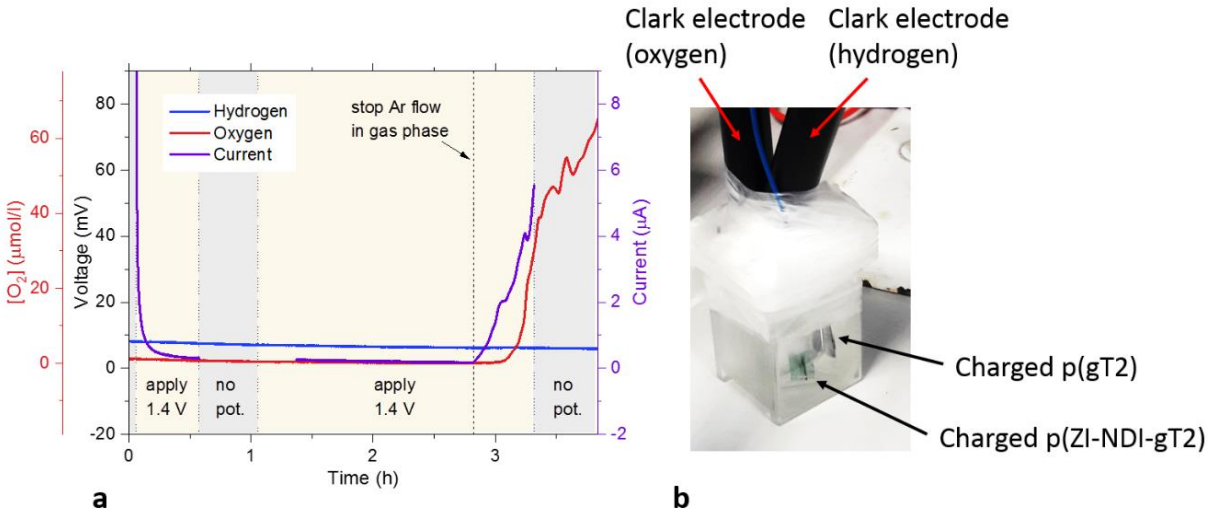


Figure S49. a) Detection of hydrogen and oxygen in 0.1 M NaCl and chronoamperometric current response under the different indicated conditions (1.4 V; no applied potential; with/without argon flow in the gas phase). b) Electrochemical cell setup including the hydrogen and oxygen sensitive Clark electrodes.

## 13.5 Hydrogen peroxide detection

Oxygen can be reduced to form hydrogen peroxide. There are two potential side reactions where oxygen can reduce p(gT2) or the reduced p(ZI-NDI-gT2) can reduce oxygen to become descharged.

Reduction of oxygen:

$$O_2 + 2H_3O^+ + 2e^- \rightarrow H_2O_2 + 2H_2O$$

Oxidation of p(gT2):

$$p(gT2) + H_3O^+ + \frac{1}{2}O_2 + NaCl \leftrightarrow p(gT2)^+\{Cl\}^- + \frac{1}{2}H_2O_2 + Na^+ + H_2O$$

Reduction of p(ZI-NDI-gT2):

$$p(ZINDIgT2)^-\{Na^+\} + H_3O^+ + \frac{1}{2}O_2 + Cl^- \leftrightarrow p(ZINDIgT2) + \frac{1}{2}H_2O_2 + NaCl + H_2O$$

Procedure for the detection of hydrogen peroxide with peroxidase/3,3′,5,5′-tetramethylbenzidine

5.6 mg 3,3′,5,5′-tetramethylbenzidine was dissolved in 10 mL of a 0.5 M HCl (dye solution). 5 mL of 0.1 M NaCl aqeuous solution was used as the supporting electrolyte. After charging the electrochemical cell to 1.4 V for 200 seconds in ambient conditions, the solution was transfered into a cuvette (colorless solution, baseline). Then, 1 mL of a solution made of 0.04 mg/mL peroxidase from horseradish in deionised water was added and the spectra were recorded every 10 s.

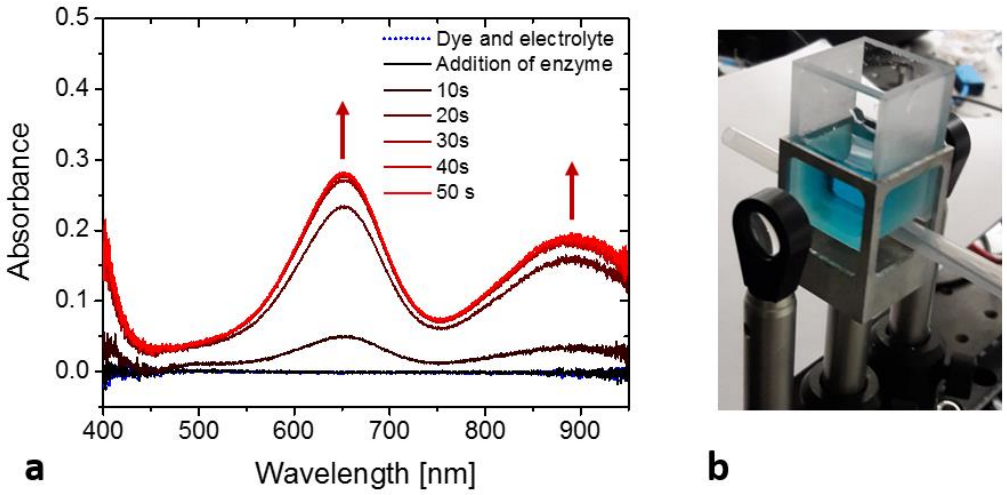


Figure S50. a) Color change of 3,3′,5,5′-Tetramethylbenzidine in the presence of peroxidase and hydrogen peroxide formed during electrochemical charging of the cell in the presence of oxygen. b) color of the oxidised dye after addition of the enyzme.

## 13.6 Charging rate and stability of the electrochemical cell

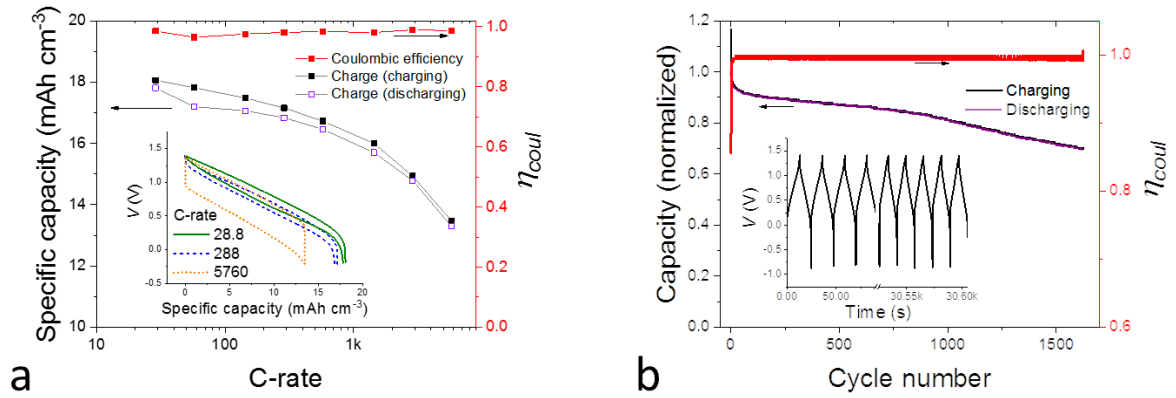


Figure S51. Galvanostatic and stability measurements on thin film p(gT2)/p(ZI-NDI-gT2) two electrode cell. (a) Specific capacity and coulombic efficiency as a function of C-rate (inset shows the galvanostatic charge-discharge curves at different C-rates). (b) Normalized specific capacity of the two-electrode cell and coulombic efficiency measured as a function of cycle number. The measurement was performed using Galvanostatic cycling at approximately 300 C-rate (inset showing the first and last cycles of the experiment).

## 13.7 Capacity recovery

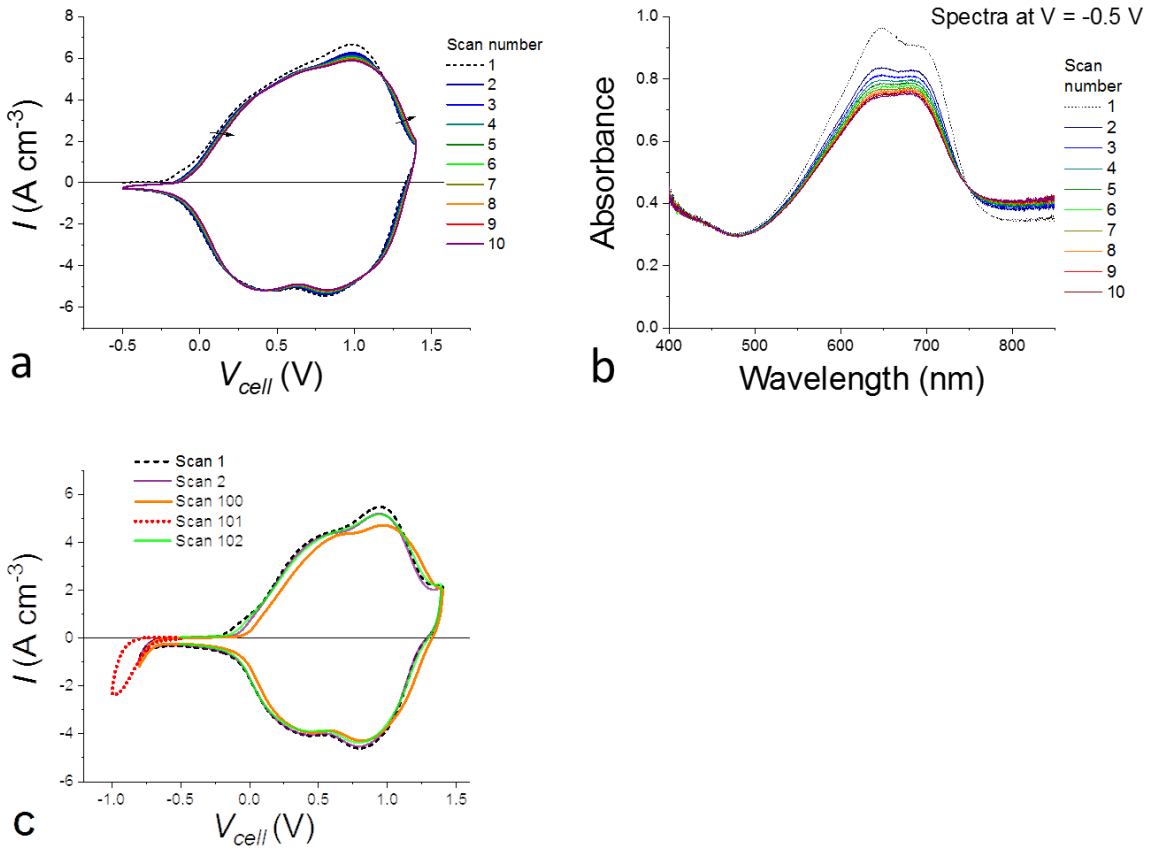


Figure S52. Probing retention limitations using spectroelectrochemistry. (a) Cyclic voltammetry measurements performed on the (p(gT2) / 0.1 M NaCl / p(ZI-NDI-gT2)) two electrode cell. (b) Optical absorbance of the two-electrode cell measured at the beginning of each scan. The features observed in cyclic voltammetry measurements shift in potential upon continuous cycling. The optical spectra shown in (b) suggests that the two polymers are in different charged stated at the beginning of each scan. We conclude that as a result of the loss of charges in the n-type polymer, the p-type polymer accumulates holes which cannot leave the film since there are not enough electrons on the anode of the cell. (c) Capacity recovery for the electrochemcal cell obtained after 100 cycles by applying a negative voltage at which p(gT2) can be reduced. The next measurement (scan 102) shows a cyclic voltammogram that is comparable to the second cycle.

## Supporting References


1 C. M. Cardona, W. Li, A. E. Kaifer, D. Stockdale and G. C. Bazan, *Adv. Mater.*, **23**, 2367–2371.

2 C. B. Nielsen, A. Giovannitti, D.-T. Sbircea, E. Bandiello, M. R. Niazi, D. A. Hanifi, M. Sessolo, A. Amassian, G. G. Malliaras, J. Rivnay and I. McCulloch, *J. Am. Chem. Soc.*, 2016, **138**, 10252–10259.

3 Gaussian 16, Revision A.03, M. J. Frisch, G. W. Trucks, H. B. Schlegel, G. E. Scuseria, M. A. Robb, J. R. Cheeseman, G. Scalmani, V. Barone, G. A. Petersson, H. Nakatsuji, X. Li, M. Caricato, A. V. Marenich, J. Bloino, B. G. Janesko, R. Gomperts, B. Mennucci, H. P. Hratchian, J. V. Ortiz, A. F. Izmaylov, J. L. Sonnenberg, D. Williams-Young, F. Ding, F. Lipparini, F. Egidi, J. Goings, B. Peng, A. Petrone, T. Henderson, D. Ranasinghe, V. G. Zakrzewski, J. Gao, N. Rega, G. Zheng, W. Liang, M. Hada, M. Ehara, K. Toyota, R. Fukuda, J. Hasegawa, M. Ishida, T. Nakajima, Y. Honda, O. Kitao, H. Nakai, T. Vreven, K. Throssell, J. A. Montgomery, Jr., J. E. Peralta, F. Ogliaro, M. J. Bearpark, J. J. Heyd, E. N. Brothers, K. N. Kudin, V. N. Staroverov, T. A. Keith, R. Kobayashi, J. Normand, K. Raghavachari, A. P. Rendell, J. C. Burant, S. S. Iyengar, J. Tomasi, M. Cossi, J. M. Millam, M. Klene, C. Adamo, R. Cammi, J. W. Ochterski, R. L. Martin, K. Morokuma, O. Farkas, J. B. Foresman, and D. J. Fox, Gaussian, Inc., Wallingford CT, 2016.

4 D. Trefz, A. Ruff, R. Tkachov, M. Wieland, M. Goll, A. Kiriy and S. Ludwigs, *J. Phys. Chem. C*, 2015, **119**, 22760–22771.

5 L. Francàs, E. Burns, L. Steier, H. Cha, L. Solà-Hernández, X. Li, P. Shakya Tuladhar, R. Bofill, J. García-Antón, X. Sala and J. R. Durrant, *Chem. Commun.*, 2018, **54**, 5732–5735.